Magnetic catalysis in even-flavor three-dimensional QED

K. Farakos and G. Koutsoumbas

Department of Physics, National Technical University of Athens, Zografou Campus, 157 80 Athens, Greece

N. E. Mavromatos

CERN, Theory Division, Geneva 23 CH-1211, Switzerland
and Department of Physics, Theoretical Physics, University of Oxford, 1 Keble Rd., OX1 3NP Oxford, United Kingdom

Arshad Momen

Department of Physics, Theoretical Physics, University of Oxford, 1 Keble Rd., OX1 3NP Oxford, United Kingdom

In this paper, we discuss the role of an external magnetic field on the dynamically generated fermion mass in even-flavor QED in three space-time dimensions. Based on some reasonable approximations, we present analytic arguments on the fact that, for weak fields, the magnetically induced mass increases quadratically with increasing field, while at strong fields one crosses over to a mass scaling logarithmically with the external field. We also confirm this type of scaling behavior through quenched lattice calculations using the non-compact version for the gauge field. Both the zero and finite temperature cases are examined. A preliminary study of the fermion condensate in the presence of magnetic flux tubes on the lattice is also included.

I. INTRODUCTION

The particle mass generation via dynamical symmetry breaking has been a much-studied scenario in particle physics as well as in condensed-matter systems. In recent years this phenomenon has been studied in the presence of background fields, such as constant external magnetic fields [1–9], following and extending the formalism developed by Schwinger [10]. The formalism has been applied to models that had gauge and/or four-fermion interactions. It was found that such constant background configurations can enhance the dynamical symmetry breaking by driving the critical coupling to a smaller value and thus catalyzing the symmetry breaking. A concrete example of this phenomenon, of relevance to us in this work, is the dynamical chiral symmetry breaking of chiral symmetry in massless QED (in three and four dimensions) in the presence of an external magnetic field [1,2,6–8] where the dynamically generated fermion mass depends on the value of the external field.

The magnetically catalyzed mass generation in $(2+1)$-dimensional QED may have interesting condensed-matter applications [7,8], given the suggestions that high-temperature superconductors can be described effectively by field theories such as three-dimensional QED (QED_3) [11] or by non-Abelian gauge models based on the group $SU(2) \times U(1)$ [12,7][1]. Indeed, there is experimental evidence for the opening of a second (superconducting) gap at the nodes of the gap in certain d-wave superconductors in the presence of strong external magnetic fields [13]. As remarked in [14], in the context of condensed-matter-inspired

models, the scaling of the thermal conductivity with the external field is different between the gauge [7,8] and four-fermion theories [15]. Thus, a detailed study of the magnetically-induced chiral symmetry breaking phenomenon in the context of QED_3 is phenomenologically desirable, given that such studies may lead to more detailed experiments in the spirit of [13], that can probe deep in the structure of the novel high-temperature superconductors.

In $2+1$ dimensions chiral symmetry can be defined only if the number of fermion flavors is even [16]. This fact is relevant for a planar high-T_c superconducting antiferromagnetic system [11,17] which comprises of two sublattices. Within a generalized [12] spin-charge separation framework [18], there will be two species of charged fermion excitations (called holons), one associated with each sublattice [11,12]. Finally, the $(2+1)$-dimensional theory with even number of fermion flavors [7] can be viewed as a dimensional reduction of the four-dimensional effective Lagrangian of [5].

In QED_3, the magnetic catalysis of the chiral symmetry breaking for strong external fields is established by looking at the Schwinger-Dyson equations [6,7]. In these works the Landau level formalism was used to truncate the fermion propagators to the lowest Landau level. This formalism is satisfactory for certain aspects of the magnetic catalysis for strong magnetic fields [7], but for weak fields the result can definitely be questioned, given that in that case the spacing between Landau levels becomes small, and one effectively deviates from the lowest Landau level description. Recently two of us [19] have looked at the role of higher Landau levels and showed that they contribute by inducing a (parity-violating) magnetic moment which scales with the applied magnetic field. Moreover, the role of higher Landau levels in inducing a critical temperature even in the free fermion case, under certain circumstances, was emphasized in [8]. For all of the above reasons it is important to incorporate the effects of *all* the higher Landau levels in the Schwinger-Dyson for-

---

[1]The relativistic (Dirac) nature of the fermion fields is justified by the fact that they describe the excitations about the *nodes* of a d-wave superconducting gap.

malism, avoiding the use of the mean field Landau level decomposition altogether. This is what we shall attempt to do in the first (analytic) part of this paper. We shall compare these results by performing some preliminary (quenched) lattice analyses in the second part of the paper. In the latter respect we have to mention that the quenched approximation for fermions employed here allows for the ladder gauge quantum fluctuations in the fermion free energy to be incorporated, but prevents the use of internal fermion loops, as the treatment of the latter requires an algorithm for treating dynamical fermions which is currently under construction.

The paper is organized as follows. In Sec. II we give a brief review of the $SU(2) \times U_S(1)$ model of [12], as well as the Dirac algebra in three-dimensional spacetime with an even number of fermion flavors. In Sec. III we review the Schwinger-Dyson (SD) equation for the fermion propagator in the absence of the the external magnetic field. In Sec. IV we present the results for the case of strong external fields, where a logarithmic scaling of the induced condensate with the external magnetic field occurs. In Sec. V we present the SD equations for the weak magnetic fields ignoring the photon polarization to make contact with the lattice result presented in the second half of the paper. We show that under certain approximations, the scaling behavior of the condensate with the external magnetic field can be found. In the next section, we attempt to go beyond the quenched approximation analytically, by including the photon polarization and modify accordingly the Schwinger-Dyson equations. The analysis becomes very complicated to be handled analytically for finite temperatures, and this is the reason why we turn to the lattice formulation of the problem in Sec. VII, where we set up the formalism and relevant notations. In Sec. VIII the lattice results are presented for both zero and finite temperatures; in addition, a preliminary extension of the results to the non-uniform magnetic field cases is attempted by examining the magnetic catalysis phenomenon in the case of flux tubes. This model may constitute a prototype for the study of the effects of electromagnetic vortices in condensed matter systems, which are of relevance to high-temperature superconductivity. Conclusions and outlook are presented in Sec. IX.

II. THE MODEL AND ITS SYMMETRIES

The $SU(2) \times U(1)$ model of [20] is a toy model for dynamical electroweak gauge symmetry breaking in three dimensions, while in the context of condensed-matter systems, the $SU(2) \times U_S(1)$ model of [12] is based on a gauged *particle-hole symmetry*, via a suitable extension of the spin-charge separation [18]. The holons transform as a doublet under the $SU(2)$ (particle-hole) symmetry. In this respect the model is different from other $SU(2) \times U(1)$ spin-charge separated theories, which are based on either direct gauging of genuine spin rotation $SU(2)$ symmetries [21], or non-Abelian bosonization techniques [22,23]. The phase diagram of the model of [12], and the associated symmetry-breaking patterns, are quite different from these other models.

The three-dimensional continuum Lagrangian of the model is given (in Euclidean metric, which we use hereafter) by [20,7],

$$\mathcal{L} = -\frac{1}{4}(F_{\mu\nu})^2 - \frac{1}{4}(\mathcal{G}_{\mu\nu})^2 + \bar{\Psi}_i D_\mu \gamma_\mu \Psi_i - m \bar{\Psi}_i \Psi_i \tag{2.1}$$

where $D_\mu = \partial_\mu - i g_1 a_\mu^S - i g_2 \sigma^a B_{a,\mu}$, and $F_{\mu\nu}$, $\mathcal{G}_{\mu\nu}$ are the corresponding field strengths for an abelian (''statistical'') $U_S(1)$ gauge field a_μ^S and a non-abelian (''spin'') SU(2) gauge field B_μ^a, respectively. Because of the antiferromagnetic nature of the condensed matter system the fermions Ψ_i are four-component spinors, $i = 1, \cdots N$. We note that Ψ_i may be written as

$$\Psi_i \equiv \begin{pmatrix} \Psi_{i1} \\ \Psi_{i2} \end{pmatrix}. \tag{2.2}$$

Then the Lagrangian decomposes into two parts, one for Ψ_{i1} and one for Ψ_{i2}, which will be called ''fermion species'' in the sequel. The presence of the even number of fermion species allows us to define chiral symmetry and parity in three dimensions [16], which we discuss below. The bare mass m term is parity conserving and has been added by hand in the Lagrangian (2.1). In the model of [12,7], this term is generated dynamically via the formation of the fermion condensate $\langle \bar{\Psi} \Psi \rangle$ by the strong $U_S(1)$ coupling. However, for our purposes, the details of the dynamical mass generation is not important and hence it will be sufficient to include a bare mass term for the holons representing the mass generated by the (strongly coupled) $U_S(1)$ interactions in the superconducting phase.

In what follows we shall ignore for simplicity the non-Abelian gauge group structure and concentrate only in the Abelian model in the presence of an *external* electromagnetic field, which should not be confused with the statistical Abelian gauge field $U_S(1)$. The incorporation of the gauged $SU(2)$ structure leads to a much richer phase structure [24,19] and we reserve the discussion for future publication.

For even-flavor models a convenient representation for the γ_μ, $\mu = 0,1,2$, matrices is the reducible 4×4 representation of the Dirac algebra in three dimensions [16]:

$$\gamma^0 = \begin{pmatrix} i\boldsymbol{\sigma}_3 & \mathbf{0} \\ \mathbf{0} & -i\boldsymbol{\sigma}_3 \end{pmatrix} \quad \gamma^1 = \begin{pmatrix} i\boldsymbol{\sigma}_1 & \mathbf{0} \\ \mathbf{0} & -i\boldsymbol{\sigma}_1 \end{pmatrix}$$

$$\gamma^2 = \begin{pmatrix} i\boldsymbol{\sigma}_2 & \mathbf{0} \\ \mathbf{0} & -i\boldsymbol{\sigma}_2 \end{pmatrix} \tag{2.3}$$

where $\boldsymbol{\sigma}$ are 2×2 Pauli matrices and the (continuum) spacetime is taken to have Euclidean signature.

As well known [16] there exist two 4×4 matrices which anticommute with γ_μ, $\mu = 0,1,2$:

$$\gamma_3 = \begin{pmatrix} 0 & \mathbf{1} \\ \mathbf{1} & 0 \end{pmatrix}, \quad \gamma_5 = i \begin{pmatrix} 0 & \mathbf{1} \\ -\mathbf{1} & 0 \end{pmatrix} \tag{2.4}$$

where the substructures are 2×2 matrices. These are the generators of the ''chiral'' symmetry for the massless-fermion theory:

$$\Psi\rightarrow\exp(i\theta\gamma_3)\Psi$$

$$\Psi\rightarrow\exp(i\omega\gamma_5)\Psi. \qquad (2.5)$$

Note that these transformations do not exist in the fundamental two-component representation of the three-dimensional Dirac algebra, and therefore the above symmetry is valid for theories with even fermion species only.

For later use we note that the Dirac algebra in $(2+1)$ dimensions satisfies the identity:

$$\gamma^\mu\gamma^\nu=-\delta^{\mu\nu}-\tau_3\epsilon^{\mu\nu\lambda}\gamma^\lambda;\quad \tau_3\equiv i\gamma_3\gamma_5=\begin{pmatrix}\mathbf{1}&0\\0&-\mathbf{1}\end{pmatrix}$$

$$\gamma^\mu\gamma^\lambda\gamma^\mu=\gamma^\lambda$$

$$\gamma^\mu\gamma^0\gamma^i\gamma^j\gamma^\mu=-\delta^{ij}\gamma^0-3\tau_3\epsilon^{ij}$$

$$\gamma^\mu\gamma^i\gamma^j\gamma^\mu=-3\delta^{ij}-\tau_3\gamma^0\epsilon^{ij}$$

$$\gamma^\mu\gamma^j\gamma^i\gamma^k\gamma^\mu=-\delta^{ij}\gamma^k-\delta^{ik}\gamma^j+\delta^{jk}\gamma^i \qquad (2.6)$$

which is specific to three dimensions only. Here the Greek indices are space time indices, and repeated indices denote summation.

Parity in this formalism is defined as the transformation

$$P:\ \Psi(x^0,x^1,x^2)\rightarrow-i\gamma^3\gamma^1\Psi(x^0,-x^1,x^2) \qquad (2.7)$$

and it is easy to see that a parity-invariant mass term for Ψ amounts to masses with *opposite* signs between the two species [16], while a parity-violating one corresponds to masses of equal signs.

The set of generators

$$\mathcal{G}=\{\mathbf{1},\gamma_3,\gamma_5,\Delta\equiv i\gamma_3\gamma_5\} \qquad (2.8)$$

form [20,12] a global $U(2)\simeq SU(2)\times U_S(1)$ symmetry. The identity matrix $\mathbf{1}$ generates the $U_S(1)$ subgroup, while the other three form the SU(2) part of the group. The currents corresponding to the above transformations are

$$J_\mu^\Gamma=\bar{\Psi}\gamma_\mu\Gamma\Psi\quad \Gamma=\gamma_3,\gamma_5,i\gamma_3\gamma_5 \qquad (2.9)$$

and are *conserved* in the *absence* of a fermionic *mass* term. It can be readily verified that the corresponding charges $Q_\Gamma\equiv\int d^2x\Psi^\dagger\Gamma\Psi$ lead to an $SU(2)$ algebra [20]:

$$[Q_3,Q_5]=2iQ_\Delta\quad [Q_5,Q_\Delta]=2iQ_3$$

$$[Q_\Delta,Q_3]=2iQ_5. \qquad (2.10)$$

In the presence of a mass term, these currents are not conserved:

$$\partial^\mu J_\mu^\Gamma=2m\bar{\Psi}\Gamma\Psi, \qquad (2.11)$$
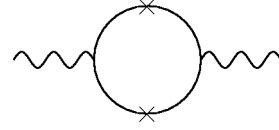

FIG. 1. One-loop vacuum polarization for photons (wavy lines) in QED$_3$. The solid lines with crosses represent fermions in the presence of an external magnetic field.

while the current corresponding to the generator $\mathbf{1}$ is *always* conserved, even in the presence of a fermion mass. The situation is parallel to the treatment of the $SU(2)\times SU(2)$ chiral symmetry breaking in low-energy QCD and the partial conservation of axial current (PCAC). The bilinears

$$\mathcal{A}_1\equiv\bar{\Psi}\gamma_3\Psi,\quad \mathcal{A}_2\equiv\bar{\Psi}\gamma_5\Psi,\quad \mathcal{A}_3\equiv\bar{\Psi}\Psi$$

$$B_{1\mu}\equiv\bar{\Psi}\gamma_\mu\gamma_3\Psi,\quad B_{2\mu}\equiv\bar{\Psi}\gamma_\mu\gamma_5\Psi,\quad B_{3\mu}\equiv\bar{\Psi}\gamma_\mu\Delta\Psi,$$

$$\mu=0,1,2 \qquad (2.12)$$

transform as *triplets* under $SU(2)$. The $SU(2)$ singlets are

$$\mathcal{A}_4\equiv\bar{\Psi}\Delta\Psi,\quad B_{4,\mu}\equiv\bar{\Psi}\gamma_\mu\Psi \qquad (2.13)$$

i.e. the singlets are the parity violating mass term, and the four-component fermion number.

We now notice that in the case where the fermion condensate $\mathcal{A}_3$ is generated dynamically, energetics prohibits the generation of a parity-violating gauge invariant $SU(2)$ term [25], and so a parity-conserving mass term necessarily breaks [7] the $SU(2)$ group down to a τ_3-$U(1)$ sector [11], generated by the σ_3 Pauli matrix in two-component notation. Upon coupling the system to external electromagnetic potentials, this phase with massive fermions shows *superconductivity*. The superconductivity is strongly type II [11,7] as the Meissner penetration depth of external magnetic fields turn out to be very large,[2] and hence the study of the response of the system to the external electromagnetic fields is justified (see Fig. 1).

III. THE SCHWINGER-DYSON EQUATION FOR THE FERMION

QED$_3$ is a super-renormalizable theory which is confining in the infrared regime. Accordingly, it acts as a simple prototype for the analysis of the chiral symmetry breaking in QCD. The standard tools for investigating the chiral symmetry breaking are the celebrated Schwinger-Dyson equations. In this section, let us set up the Schwinger-Dyson equations for the fermion propagator (see Fig. 2).

The Schwinger-Dyson equation concerning the fermion propagator $S_F(p)$ (for zero bare fermion mass) is given by

---

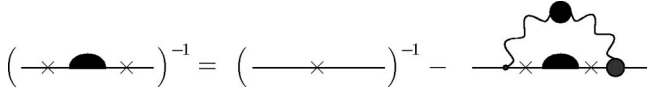[2]The high-temperature superconducting oxides are strongly type II superconductors.

FIG. 2. The Schwinger-Dyson equation for the fermion self-energy. The curly line indicates the $U_S(1)$ statistical photon. Solid lines with crosses represent fermions in the presence of the external magnetic field. Blobs indicate quantum corrections (loops), which are ignored in the ladder approximation. Quantum dynamics of the electromagnetic field has been suppressed.

$$S_F^{-1}(p) = \gamma \cdot p - g \int \frac{d^3k}{(2\pi)^3} \gamma^\mu S_F(k) \Gamma^\nu(k, p-k) D_{\mu\nu}(p-k) \tag{3.1}$$

where Γ^ν is the fermion-photon vertex function and $D_{\mu\nu}$ is the exact photon propagator. However, to this order, let us make the following approximations:

(1) Use the bare vertex function, namely

$$\Gamma^\nu(k, p-k) = g\gamma^\nu, \tag{3.2}$$

so that the gap equation reads

$$S_F^{-1}(p) = \gamma \cdot p - g^2 \int \frac{d^3k}{(2\pi)^3} \gamma^\mu S_F(k) \gamma^\nu(k, p-k)$$

$$\times D_{\mu\nu}(p-k). \tag{3.3}$$

(2) Now, we choose the following ansatz for the *full* fermion propagator:

$$S_F^{-1}(p) = A(p)\gamma^0 p_0 + B(p)\boldsymbol{\gamma \cdot p} + \Sigma(p). \tag{3.4}$$

Using this ansatz, let us now perform a trace over the gamma matrices in Eq. (3.1). This gives us the following gap equation:

$$\Sigma(p) = g^2 \int \frac{d^3k}{(2\pi)^3} \frac{\Sigma(k)}{A^2 k_0^2 + B^2 \boldsymbol{k}^2 + \Sigma^2(k)} \sum_\mu D_{\mu\mu}(p-k). \tag{3.5}$$

(3) To further simplify the gap equation let us use the zeroth order result for the wavefunction renormalization, namely $A(p) = B(p) = 1$, which is often justified in the large N argument [16] (see however [27]) so that Eq. (3.5) reads

$$\Sigma(p) = g^2 \int \frac{d^3k}{(2\pi)^3} \frac{\Sigma(k)}{[k_0^2 + \boldsymbol{k}^2 + \Sigma^2(k)]} D_{\mu\mu}(p-k). \tag{3.6}$$

(4) The photon propagator $D_{\mu\nu}(k)$ can be replaced by the ladder resummed propagator which can be justified in the large-N limit. The resummed propagator (in the absence of the magnetic field) is given by

$$D_{\mu\nu}(p) = \frac{\left(\delta_{\mu\nu} - \dfrac{p_\mu p_\nu}{p^2}\right)}{p^2(1 - \Pi(p))} = \frac{\left(\delta_{\mu\nu} - \dfrac{p_\mu p_\nu}{p^2}\right)}{p^2\left(1 + \dfrac{g^2}{8p}\right)}. \tag{3.7}$$

The gap equation thus obtained in the absence of the magnetic field can be solved using the bifurcation method [16]. There are two solutions namely,

$$\Sigma_1(p) \sim p^{-8/\pi^2 N}, \quad \Sigma_2(p) \sim p^{1 - 8/\pi^2 N} \tag{3.8}$$

where N is the (large) number of fermion flavors. However, it is natural to expect that these solutions will change in the presence of the external magnetic field; we will discuss this generalization in the following sections.

IV. THE DYNAMICALLY GENERATED FERMION MASS AT STRONG MAGNETIC FIELDS

As mentioned above, hereafter we consider only the Abelian gauge group $U_S(1)$ in the presence of an external electromagnetic potential A_μ^{ext}, corresponding to a constant magnetic field **B**, perpendicular to the spatial plane. The dynamics is described by the Lagrangian

$$\mathcal{L} = -\frac{1}{4}(F_{\mu\nu})^2 + \bar{\Psi} D_\mu \gamma_\mu \Psi - m\bar{\Psi}\Psi \tag{4.1}$$

where $D_\mu = \partial_\mu - iga_\mu^S - ieA_\mu^{ext}$. The mass m here should be viewed as an (infrared) regulator mass. In the dynamical mass generation scenario investigated below via the SD method m should be set to zero, given that the dynamics of the gauge field and the magnetic field are both responsible for the appearance of a mass in the fermion propagator. For the lattice analysis, on the other hand, the presence of an initial small ''bare'' regulating mass $m \neq 0$ appears necessary [8].

We commence our analysis by noting that the presence of an external magnetic field, perpendicular to the spatial plane $x_1 x_2$, breaks Lorentz and translational invariance. The configuration space form of the fermion two-point function $G(x, y)$ for the three-dimensional problem at hand has the generic form [6]:

$$G(x, y) = \exp\left(\frac{ie}{2}(x-y)^\mu A_\mu^{ext}(x+y)\right) \widetilde{G}(x-y) \tag{4.2}$$

where A_μ^{ext} denotes the external electromagnetic potential, corresponding to a constant homogeneous magnetic field perpendicular to the spatial plane $x_1 x_2$: $A_\mu^{ext} = (0, -(B/2)x_2, (B/2)x_1)$ (in an obvious notation). The field-dependent phase factor in Eq. (4.2) breaks translational invariance, implying that, in general, $G(x, y)$ does not admit a Fourier transform expressible in terms of a single momentum (vector) variable $\boldsymbol{k}$.

The translationally-invariant part $\widetilde{G}(x-y)$ has a Fourier transform $\widetilde{S}_F(k)$ of the form [10]

$$\tilde{S}_F(k) = i \int_0^\infty ds\, e^{-s(k_0^2 + m^2 + \mathbf{k}^2 (\tanh z/z))} [(m - \gamma \cdot k)$$

$$- i(\gamma_1 k_2 - \gamma_2 k_1)\tanh z](1 - i\gamma_1 \gamma_2 \tanh z)$$

$$(4.3)$$

where m is the mass of the fermion, and $z = seB$. Note that we are distinguishing between the coupling constant g for the

statistical $U(1)$ gauge field and the electromagnetic charge e. The Schwinger propagator admits the following expansion in terms of the Landau levels [26]:

$$\tilde{S}_F(k) \equiv i e^{-\mathbf{k}^2/eB} \sum_{n=0}^\infty \frac{(-1)^n D_n(k_0, \mathbf{k})}{k_0^2 + m^2 + 2enB}, \quad B \neq 0, \quad (4.4)$$

with

$$D_n(k_0, \mathbf{k}) \equiv (m - \gamma_0 k_0) \left[(1 - i\gamma_1 \gamma_2) L_n\!\left(\frac{2\mathbf{k}^2}{eB}\right) - (1 + i\gamma_1 \gamma_2) L_{n-1}\!\left(\frac{2\mathbf{k}^2}{eB}\right) \right] + 4(\gamma \cdot k) L_{n-1}^1\!\left(\frac{2\mathbf{k}^2}{eB}\right) \qquad (4.5)$$

$$= (m - \gamma_0 k_0) \left[L_n^{-1}\!\left(\frac{2\mathbf{k}^2}{eB}\right) + i\tau_3 \gamma_0 \!\left(L_n\!\left(\frac{2\mathbf{k}^2}{eB}\right) + L_{n-1}\!\left(\frac{2\mathbf{k}^2}{eB}\right) \right) \right] + 4(\gamma \cdot k) L_{n-1}^1\!\left(\frac{2\mathbf{k}^2}{eB}\right). \qquad (4.6)$$

For QED$_3$ the scaling of the dynamically generated fermion mass with the external magnetic field had been discussed by Shpagin [6] and two of us [7]. Let us begin with the case when the external magnetic field is very strong. As stated in the Introduction, in this case it is sufficient to truncate the fermion propagator [in the absence of the $U_S(1)$ interactions] to the lowest Landau level (4.4), so that we get

$$\tilde{S}_F^{LLL}(k) = i e^{-\mathbf{k}^2/eB} \frac{1}{m + \gamma^0 k^0} (1 - i\gamma^1 \gamma^2). \qquad (4.7)$$

As we will be dealing with the lowest Landau levels only, it is expedient to choose the ansatz for the "exact" propagator for the lowest Landau level fermions to be of the form

$$S_F^{LLL}(k) = i e^{-\mathbf{k}^2/eB} \frac{1}{\Sigma(k) + A(k)\gamma^0 k^0} (1 - i\gamma^1 \gamma^2). \qquad (4.8)$$

Hence, following [6], the gap equation for the lowest Landau level fermion is given by

$$\Sigma(p) = g^2 \int \frac{d^3 k}{(2\pi)^3} e^{-\mathbf{k}^2/eB} \frac{\Sigma(k)}{A^2 k_0^2 + \Sigma^2(k)} D_{00}(p - k). \qquad (4.9)$$

According to [6] the photon vacuum polarization gets suppressed as $1/\sqrt{eB}$ at strong magnetic fields and the photons become almost free. Thus in the strong field limit the photon propagator is given in the Landau gauge by the expression

$$D_{\mu\nu}(p) = \frac{\delta_{\mu\nu} - \dfrac{p_\mu p_\nu}{p^2}}{p^2} \cdot \frac{1}{p^2 \left(1 + 0.14037 \dfrac{g^2}{\sqrt{eB}}\right)}. \qquad (4.10)$$

Accordingly, we have

$$\Sigma(p) = \tilde{g}^2 \int d^2 k\, e^{-\mathbf{k}^2/eB} \frac{1}{(p - k)^2}$$

$$\times \left(1 - \frac{(p_0 - k_0)^2}{(p - k)^2} \right) \int \frac{dk_0}{(2\pi)^3} \frac{\Sigma(k)}{A^2 k_0^2 + \Sigma^2(k)}, \qquad (4.11)$$

where $\tilde{g}^2 \equiv g^2/[1 + 0.14037(g^2/\sqrt{eB})]$. Let us set p to zero. Then,

$$\Sigma(0) = \tilde{g}^2 \int e^{-\mathbf{k}^2/eB} \mathbf{k}^2 \frac{d^2 \mathbf{k}}{(k_0^2 + \mathbf{k}^2)^2} \int \frac{dk_0}{(2\pi)^3} \frac{\Sigma(k)}{A^2 k_0^2 + \Sigma^2(k)}. \qquad (4.12)$$

For strong fields $eB \to \infty$, we suppose that setting $\Sigma(k) \approx \Sigma(0)$ and $A \approx 1$ yield a sufficiently good approximation [27]. Setting $\mathbf{k}^2 \equiv x$, the gap equation becomes

$$1 = \frac{\tilde{g}^2}{8\pi^2} \int dk_0 \int dx\, e^{-x/eB} \frac{x}{(k_0^2 + x)^2} \frac{1}{k_0^2 + \Sigma^2(0)}. \qquad (4.13)$$

Assuming that the dynamically generated fermion mass is much smaller than the external magnetic field, i.e. $\Sigma(0) \ll \sqrt{eB}$, we cut off the x integration by $\sqrt{eB}$ and after the k_0 integration we get the transcendental equation

$$\Sigma(0) \approx \frac{\tilde{g}^2}{4\pi} \int_{\Sigma(0)}^{\sqrt{eB}} dy\, e^{-y^2/eB} \left(\frac{2}{y} - \frac{3\Sigma(0)}{y^2} + \frac{\Sigma(0)^3}{y^4} \right). \qquad (4.14)$$

The final result reads

$$\Sigma(0) \approx 2\tilde{\alpha} \ln\!\left(\frac{\sqrt{eB}}{\Sigma(0)} \right) + O\!\left(\frac{\Sigma(0)}{\sqrt{eB}} \right), \quad \text{where} \quad \tilde{\alpha} \equiv \frac{\tilde{g}^2}{4\pi}. \qquad (4.15)$$

This equation can be solved numerically as in [7], leading to a logarithmic scaling of the induced fermion condensate with the magnetic field, $\Sigma(0) \sim \ln(\sqrt{eB}/\tilde{\alpha})$.

Note that the most important aspect of this type of behavior comes from the presence of the exponential factor in the form of the free propagator in Eq. (4.7). However, when the external magnetic field is weak, one has to include all the higher Landau levels as the levels become closely spaced. Also, the wave functions for these levels grow with momentum as they involve Laguerre polynomials. Hence, one has to work with a generic ansatz for the fermion propagator, such as Eq. (3.4). However, in view of the breaking of translational invariance by the field-dependent phase factor in Eq. (4.2), a straightforward application of this ansatz is not possible. Nevertheless, as we shall discuss below, such an ansatz can still give qualitatively correct predictions for the scaling of the induced condensate with the external field.

V. THE DYNAMICAL FERMION MASS IN WEAK EXTERNAL MAGNETIC FIELDS UNDER QUENCHED APPROXIMATION

We are looking at the leading scaling behavior with the magnetic field intensity of the dressed fermion propagator in the presence of an external magnetic field eB for the case of weak fields $eB \ll \Sigma(0)$ where $\Sigma(0) \equiv m$ is a dynamically generated mass due to the statistical $U_S(1)$ interactions in the model. Obviously, since $m \propto g^2$, whereas g denotes the coupling of these interactions, the weak field limit is achieved for relatively strong gauge interactions. However, as stated earlier, we are interested in the behavior of the system under weak magnetic fields as well and in this regime the Landau level decomposition is not particularly helpful.

This is a technically involved problem, and we shall not attempt to solve it exactly in what follows. Instead we shall make an attempt to present an *approximate* treatment, which hopefully captures the important *qualitative* features of the phenomenon. As we shall see later on, preliminary lattice calculations will support the results obtained in this section.

The main complication arises from the fact, mentioned in the previous section, that the presence of an external field, perpendicular to the spatial plane, breaks, in addition to Lorentz invariance, also translational invariance in the spatial plane. This is apparent from the configuration space form (4.2) of the fermion Green's function. The breaking of translational invariance is manifested through the field-dependent phase factor in Eq. (4.2). A Schwinger-Dyson equation for $G(x,y)$ can then be obtained as in [6], but unfortunately, due to the form (4.2), a passage to momentum space with an appropriate Fourier transform based on a single momentum variable is not feasible.

Below we shall make a modest attempt to calculate analytically the scaling behavior of the chiral condensate with the magnetic field, at least qualitatively, and then compare with the lattice results. This is possible by adopting an ansatz for the fermion propagator in momentum space, $S_F^{-1}(p)$, as if the translational invariance breaking phase factor in Eq. (4.2) was absent. Specifically, we assume that the fermion propagator in the presence of a *weak* external magnetic field

can still have a Fourier transform, based on a single momentum variable, which takes the *approximate* form

$$S_F^{-1}(p) = [A_0 + A_1 \gamma_1 \gamma_2] \gamma_0 p_0 + C \boldsymbol{\gamma} \cdot \mathbf{p} + [\Sigma_0 + \Sigma_1 \gamma_1 \gamma_2].$$
(5.1)

All the qualitative information about the effects of the external field B is encoded inside the coefficients. As we shall see later on, by comparison with the preliminary lattice results in the quenched approximation, the qualitative features of the scaling of the magnetically-induced chiral condensate with the external field seem to be correctly captured by the above ansatz. It is understood, of course, that these results should be taken with caution and viewed only as preliminary. A complete lattice analysis involving dynamical fermions, which will settle these issues, is still pending. Hopefully it will constitute the topic of a forthcoming work.

Under the above approximation, the Schwinger-Dyson equation for the fermion propagator in the massless limit assumes the form

$$S_F^{-1}(p) = \tilde{S}_F^{-1}(p)|_{m=0} - g^2 \int \frac{d^3 k}{(2\pi)^3} D_{\mu\nu}(p-k) \gamma^\mu S_F(k) \Gamma^\nu.$$
(5.2)

It is sufficient for our purposes to use the bare photon vertex ($\Gamma^\nu = \gamma^\nu$), and set the wave-function renormalization to one. These will be justified later on.

Taking the trace in the above equation, we obtain

$$4\Sigma(p) = -g^2 \int \frac{d^3 k}{(2\pi)^3} D_{\mu\nu}(p-k) \mathrm{Tr}(\gamma^\mu \tilde{S}_F(k) \gamma^\nu)$$
(5.3)

where we denoted Σ_0 by $\Sigma(p)$. A more important remark is that inside the integral we have approximated the (unknown) fermion propagator $S_F(k)$ by the form $\tilde{S}_F(k)$ of Eq. (4.3), which is the propagator in a homogeneous external magnetic field. One has

$$\mathrm{Tr}(\gamma^\mu \tilde{S}_F(k) \gamma^\nu) = \int_0^\infty ds\, e^{-s(k_0^2 + k^2(\tanh z/z) + \Sigma^2)}$$

$$\times \mathrm{Tr}[\gamma^\mu(-\boldsymbol{\gamma} \cdot k + \Sigma(k))\gamma^\nu$$

$$+ i \gamma^\mu(-\Sigma(k) + \boldsymbol{\gamma} \cdot k)\gamma_1 \gamma_2 \gamma^\nu \tanh z$$

$$- i \gamma^\mu(\gamma_1 k_2 - \gamma_2 k_1)$$

$$\times \tanh z(1 - i \gamma_1 \gamma_2 \tanh z)\gamma^\nu].$$
(5.4)

Since we work in the Landau gauge, $D_{\mu\nu}(q)$ is given by $(q^2 \delta_{\mu\nu} - q_\mu q_\nu)/q^4$. Using the following identities of the γ matrices in Euclidean space:

$$\text{Tr}(\gamma_\mu \gamma^\mu) = -12$$

$$(q \cdot \gamma)^2 = -q^2$$

$$\text{Tr}(\gamma^\mu \mathcal{O} \gamma^\nu) D_{\mu\nu}(q) = -\frac{2}{q^2} \text{Tr} \mathcal{O} \qquad (5.5)$$

where $\mathcal{O}$ is any operator, one can write Eq. (5.4) in the form

$$D_{\mu\nu}(p-k) \text{Tr}(\gamma^\mu \widetilde{S}_F(k) \gamma^\nu)$$

$$= -\frac{8}{(p-k)^2} \int_0^\infty ds \Sigma(k) e^{-s(k_0^2 + \boldsymbol{k}^2 (\tanh z / z) + \Sigma^2(k))}.$$

$$(5.6)$$

Using Eq. (5.6), Eq. (5.3) becomes

$$\Sigma(p) = \frac{2g^2}{(2\pi)^3} \int_0^\infty ds \int \frac{d^3 k}{(k-p)^2} \Sigma(k) e^{-s(k_0^2 + \boldsymbol{k}^2 (\tanh z / z) + \Sigma^2(k))}.$$

$$(5.7)$$

Setting $p=0$ and approximating $\Sigma(k) \simeq \Sigma(0) \equiv m$ in the integrand yields

$$1 = \frac{2g^2}{(2\pi)^3} \int_0^\infty ds \int d^3 k \frac{1}{k_0^2 + \boldsymbol{k}^2} e^{-s(k_0^2 + \boldsymbol{k}^2 (\tanh z / z) + m^2)}.$$

$$(5.8)$$

Now we use the parametrization: $k_0 = k \cos\theta$, $\boldsymbol{k}^2 = k^2 \sin^2\theta$, and get

$$1 = \frac{g^2}{4\pi^{3/2}} \int_0^\infty ds \int_{-1}^{+1} dx \frac{e^{-sm^2}}{\sqrt{s\left(x^2 + (1-x^2)\dfrac{\tanh z}{z}\right)}},$$

$$(5.9)$$

with $x \equiv \cos\theta$. Then the x integration can be performed:

$$1 = \frac{1}{4\pi^{3/2}} \frac{g^2}{\sqrt{eB}}$$

$$\times \int_0^\infty dz e^{-z(m^2/eB)} \frac{1}{\sqrt{z - \tanh z}} \log \frac{\sqrt{z} + \sqrt{z - \tanh z}}{\sqrt{z} - \sqrt{z - \tanh z}}, \quad (5.10)$$

where we have set $z \equiv eBs$. At this point we define two dimensionless variables: $\mu \equiv 2\pi(m/g^2)$, $f \equiv 2\pi(\sqrt{eB}/g^2)$, and write the last equation in terms of μ and f:

$$1 = \frac{1}{2\sqrt{\pi}} \frac{1}{f} \int_0^\infty dz e^{-z(\mu^2/f^2)} \frac{1}{\sqrt{z - \tanh z}} \log \frac{\sqrt{z} + \sqrt{z - \tanh z}}{\sqrt{z} - \sqrt{z - \tanh z}}.$$

$$(5.11)$$

For each value of f the above relation gives a corresponding value for μ. The result is a universal curve $\mu(f)$, which we depict in Fig. 3 as a dashed line. This result can be translated
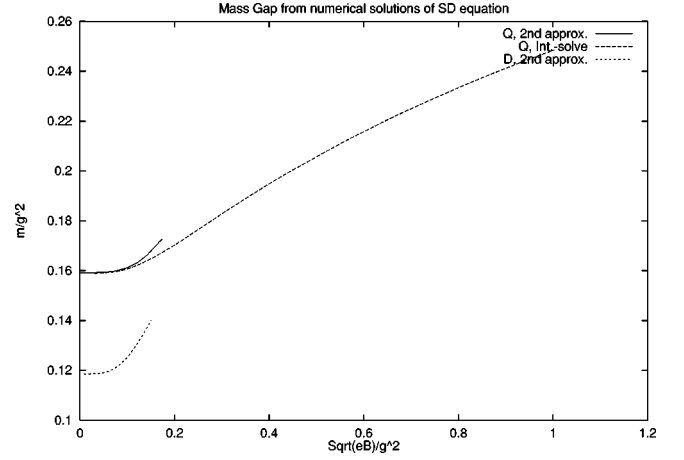

FIG. 3. Solution of Schwinger-Dyson equations for the quenched and dynamical fermions.

very easily to the language of dimensionful parameters, as well as to the lattice parameters. Notice that up to now there is no restriction to weak fields.

One may also derive an analytical approximation for the regime of weak magnetic fields. Starting from Eq. (5.8) we write the term $e^{-sk^2(\tanh z/z)}$ in the form $e^{-sk^2} \cdot e^{-sk^2(\tanh z/z - 1)}$, expand the second exponential in a power series of $z = eBs$ for weak fields and retain the terms which are at most of sixth order in eB. Then the same parametrization as before is used and the integrations over k and x are similarly carried out. Then the equation involving the integral over z is replaced by

$$1 = \frac{g^2}{2\pi} \left[\frac{1}{m} + \frac{1}{12} \frac{e^2 B^2}{m^5} - \frac{7}{48} \frac{e^4 B^4}{m^9} + \frac{773}{960} \frac{e^6 B^6}{m^{13}} + \mathcal{O}(e^8 B^8) \right].$$

$$(5.12)$$

For weak fields we may solve Eq. (5.12) by substituting the expansion $m = m_0 + m_2(eB)^2 + m_4(eB)^4 + \dots$ in Eq. (5.12) and equating the coefficients of equal powers of eB to determine the coefficients m_k. The resulting solution of Eq. (5.12) is

$$m = \frac{g^2}{2\pi} \left(1 + \frac{4\pi^4 e^2 B^2}{3g^8} - \frac{400\pi^8 e^4 B^4}{9g^{16}} + \frac{534208\pi^{12} e^6 B^6}{135 g^{24}} \right.$$

$$\left. + \mathcal{O}(e^8 B^8) \right), \qquad (5.13)$$

which may also be written as

$$\mu = 1 + \frac{1}{12} f^4 - \frac{25}{144} f^8 + \frac{8237}{8640} f^{12} + \mathcal{O}(f^{16}). \quad (5.14)$$

The above relations show that for weak magnetic fields the dynamically generated mass is quadratic in B. For somewhat bigger magnetic fields, however, the quadratic behavior is compensated by a negative quartic contribution and the increase with the magnetic field resembles very closely a linear dependence. Of course for even bigger magnetic fields higher order contributions take over.

Although we have already depicted in Fig. 3 the full solution $\mu(f)$, we also plot the solution of Eq. (5.12) [we note here that we did not actually use the solution (5.13), but rather the one which results if Eq. (5.12) is quenched to order B^2 before solving]; this is done to gain some feeling about the accuracy of the quadratic approximation, which will be the only possible approach in the case where also dynamical fermions are taken into account. The approximate solution is the full line and is restricted in the region of small B, where it is appropriate; it is quite good up to $\sqrt{eB/g^2}\approx 0.1$.

As we have just seen, in the quenched approximation one uses the free photon propagator as the fermion loops (which modifies the fermion propagator) are ignored. In the next section, we examine whether the inclusion of the photon polarization modifies the scaling behavior of the gap function with eB discussed above.

Before closing this section two important remarks are in order. First, it should be noted that the presence of the translational invariance breaking phase factors in Eq. (4.2), which have been ignored in the above treatment, will affect the numerical coefficients of the even powers of B in Eq. (5.13). This can be seen easily from the form (4.2) by an expansion in powers of the weak field B (and restriction to the real part, assuming hermiticity of the translational invariant parts). The important issue is the sign of the various terms. As we shall see later on, comparison with the (quenched) lattice results confirms the scaling with B given in Eq. (5.13), thereby justifying the above approximate method of dealing with the problem, at least for qualitative purposes. Second, the above analytic treatment, leading to Eq. (5.13), was based on the approximation of replacing $\Sigma(k)$ inside the integrals in the pertinent integral form of the gap equation by a constant $\Sigma(0)=m$, the so-called ''constant-mass approximation.'' This is sufficient for the qualitative purposes of this work, where the main interest lies on the scaling of the induced condensate with the magnetic field. It should be remarked though, that attempts to go beyond the ''constant mass approximation'' have been made in the literature, specifically in the context of three-dimensional QED in the absence of external fields [28]. The result is that the value of the induced mass m, obtained by keeping the momentum dependence of the gap function inside the pertinent integrals in the Schwinger-Dyson equation, is half the value of the mass gap obtained under the ''constant mass approximation,'' i.e. the zero-field limit ($B\rightarrow 0$) in Eq. (5.13) should be $m=g^2/4\pi$. This should be taken into account in quantitative analyses of the phenomenon, and possible detailed applications in condensed-matter physics, which, however, go beyond the scope of the present work.

VI. BEYOND THE QUENCHED APPROXIMATION

To take into account the contribution of internal fermion loops we begin with a study of the one-loop vacuum polarization graph in QED$_3$ in the case of even number of fermion flavors. The polarization tensor in the one-loop approximation is given by

$$\Pi_{\mu\nu}(p)=-g^2\int\frac{d^3k}{(2\pi)^3}\text{tr}(\gamma_\mu\widetilde{S}(k)\gamma_\nu\widetilde{S}(k-p)) \quad (6.1)$$

where $\widetilde{S}(k)$ is the fermion propagator in the presence of the external magnetic field (4.3).

The calculation of the polarization tensor is straightforward. Due to the fermionic loop, the effects of the translational invariance breaking phase factors in Eq. (4.2) *cancel*, and one can go directly to momentum space as in the zero external field situation. For our case, the photon polarization can be obtained easily by performing a dimensional reduction of the four-dimensional result [30,31]. We end up with

$$\Pi_{\mu\nu}(p)=(p^2\delta_{\mu\nu}-p_\mu p_\nu)N_0(p)+(p_\perp^2\delta_{\mu\nu}-p_{\perp\mu}p_{\perp\nu})N_1(p)$$
$$\equiv p^2 P_{\mu\nu}N_0(p)+p^2 P_{\perp\mu\nu}N_1(p), \quad (6.2)$$

where $p^2\equiv p_\perp^2$ with $p_{\perp\mu}=(0,p_1,p_2)$ and

$$N_0(p)=-\frac{g^2}{8\pi^{3/2}}\int_0^\infty\frac{ds}{\sqrt{s}}\int_{-1}^{+1}dv\,e^{-s\phi_0}\frac{z}{\sinh z}$$
$$\times[\cosh zv-v\coth z\sinh zv]$$

$$N_1(p)=-\frac{g^2}{8\pi^{3/2}}\int_0^\infty\frac{ds}{\sqrt{s}}\int_{-1}^{+1}dv\,e^{-s\phi_0}\frac{2z}{\sinh^3 z}$$
$$\times[\cosh z-\cosh zv]-N_0(p) \quad (6.3)$$

with

$$\phi_0=m^2+\frac{1-v^2}{4}p_0^2+\frac{\cosh z-\cosh zv}{2z\sinh z}p^2;$$

$$z\equiv eBs. \quad (6.4)$$

An outline of the derivation of the above-mentioned formulas is provided in the appendix.

For weak magnetic fields, we will have $\sqrt{eB}\ll\Sigma(0)$, where $\Sigma(0)$ is the dynamically generated fermion mass. Note that it is the opposite to the limit encountered in the case for the strong magnetic field [6,20]. In the weak-field limit, we can expand the above functions in a power series of $z=s\Sigma^2(0)[eB/\Sigma^2(0)]$ and take the leading and next to leading order behavior as $z\rightarrow 0$.

We have, as $z\rightarrow 0$, the following expansions to order e^2B^2:

$$\phi_0=\Sigma^2+\frac{1-v^2}{4}p^2-\frac{z^2}{48}(1-v^2)^2 p^2+O(z^4), \quad (6.5)$$

$$N_0(p)=-\frac{g^2}{8\pi^{3/2}}\int_0^\infty\frac{ds}{\sqrt{s}}\int_{-1}^{+1}dv\,e^{-s\phi_0}(1-v^2)$$
$$\times\left[1-\frac{z^2}{6}(1-v^2)\right]+O(z^4), \quad (6.6)$$

$$N_1(p) = -\frac{g^2}{8\pi^{3/2}} \int_0^\infty \frac{ds}{\sqrt{s}} \int_{-1}^{+1} dv\, e^{-s\phi_0} \frac{z^2}{12}(-3+2v^2+v^4)$$

$$+ O(z^4). \tag{6.7}$$

Note that when $z \to 0$ the term $N_1(p)$ vanishes and we recover the usual form for the polarization tensor.

To simplify the integrals, we also expand the exponential $e^{-s\phi_0}$ in a power series in z so that

$$e^{-s\phi_0} \sim e^{-s(\Sigma^2 + [(1-v^2)/4]p^2)} \left(1 + \frac{e^2 B^2 s^3}{48} (1-v^2)^2 \boldsymbol{p}^2 \right). \tag{6.8}$$

This simplifies the s-integrals. We then end up with

$$N_0(p) = -\frac{g^2}{2\pi p} \left[\left(\frac{1}{2} - \frac{2\Sigma^2}{p^2} \right) \sin^{-1}\kappa \right.$$

$$+ \frac{\Sigma}{p} - \frac{2e^2 B^2}{p^4} \left\{ \sin^{-1}\kappa - \frac{2\Sigma\kappa^2(3+2\kappa^2)}{3p} \right\}$$

$$\left. + \frac{5e^2 B^2 \boldsymbol{p}^2}{2p^6} \left\{ \sin^{-1}\kappa - \frac{2\Sigma\kappa^2(15+10\kappa^2+8\kappa^4)}{15p} \right\} \right] \tag{6.9}$$

$$N_1(p) = -\frac{g^2 e^2 B^2}{2\pi p^5} \left[\sin^{-1}\kappa - p\frac{3-\kappa^2+6\kappa^4}{6\Sigma} \right] \tag{6.10}$$

where $\kappa^2 \equiv p^2/(4\Sigma^2 + p^2)$. Note that for physical processes $0 \le \kappa \le 1$. When, $eB=0$ and $\Sigma=0$ (i.e. $\kappa=1$) we recover the known results [Eq. (3.7)], namely $N_0(p) = -g^2/8p$, $N_1(p) = 0$.

On the other hand, in the presence of the magnetic field one can readily see that in the limit $\Sigma \to 0$ the function $N_1(p)$ blows up when $\kappa \to 1$ (i.e., the massless case) due to the presence of the factor Σ in the denominator. However, for a super renormalizable theory this seems unphysical. A resolution to this puzzle can be provided by the generation of a dynamical fermion mass Σ (however small) in the presence of the magnetic field. This observation points to the magnetic catalysis even in the case for the weak fields in three-dimensional QED. Generation of such a mass would prevent the appearance of the divergences.

For $\Sigma \ne 0$, $N_0(p)$ and $N_1(p)$ behaves, when $\Sigma \ll p$ and $p \to \infty$, as

$$N_0(p) \approx -\frac{g^2}{8p} \left(1 - \frac{4e^2 B^2}{p^4} + \frac{5e^2 B^2 \sin^2\theta}{p^4} \right), \tag{6.11}$$

$$N_1(p) \approx -\frac{g^2 e^2 B^2}{2\pi p^5} \left(\frac{\pi}{2} - \frac{4p}{3\Sigma} \right) \tag{6.12}$$

where we have used the parametrization $\boldsymbol{k}^2 = k^2 \sin^2\theta$, as before. Hereafter we will be using the approximations (6.11) and (6.12) which are justified in the weak-field case.

As in the case with the quenched treatment let us proceed to get the gap equation. Again we shall adopt the approximate qualitative approach of the previous section as regards the effects of the translational invariance breaking phase factors in Eq. (4.2) due to the presence of the external field. To take account of the photon propagator, we can invoke the large-N argument to sum up the photon propagator in the ladder approximation

$$D_{\mu\nu}(p) = D^0_{\mu\nu}(p) + D^0_{\mu\kappa}(p)\Pi_{\kappa\rho}(p)D^0_{\rho\nu}(p) + \cdots \tag{6.13}$$

where $D^0_{\mu\nu}$ is the free photon propagator. To facilitate our calculations let us use the Landau gauge for the zeroth order propagator, so that

$$D^0_{\mu\nu}(p) = \frac{\delta_{\mu\nu} - \dfrac{p_\mu p_\nu}{p^2}}{p^2}. \tag{6.14}$$

Using the algebraic properties of the projectors

$$P_{\mu\nu}(p)P_{\nu\rho}(p) = P_{\mu\rho}(p)$$

$$P_{\mu\nu}(p)P_{\perp\nu\rho}(p_\perp) = P_{\perp\nu\rho}(p_\perp)$$

$$P_{\perp\mu\nu}(p_\perp)P_{\perp\nu\rho}(p_\perp) = P_{\perp\nu\rho}(p_\perp) \tag{6.15}$$

we can sum the series in Eq. (6.13) to get

$$D_{\mu\nu}(p) = \frac{1}{p^2(1-N_0(p))}$$

$$\times \left[P_{\mu\nu} + P_{\perp\mu\nu} \frac{N_1(p)\dfrac{\boldsymbol{p}^2}{p^2}}{1 - \left[N_0(p) + \dfrac{\boldsymbol{p}^2}{p^2}N_1(p) \right]} \right]. \tag{6.16}$$

To go beyond the case of quenched approximation which we discussed in the previous section, we need to include the polarization effects in our analysis treatment. To perform this improvement we replace the photon propagator in Eq. (5.3) by the ladder resummed one, given by Eq. (6.16). For the fermion propagator we proceed as we did previously for the quenched case: starting from Eq. (5.4) we expand the term $e^{-sk^2(\tanh z/z)}$ and get the expression $e^{-sk^2} \cdot e^{-sk^2(\tanh z/z - 1)}$. Then we expand the second exponential in powers of

$z = eBs$, retain the terms which are at most of second order in eB and integrate over s. Taking traces over the Dirac γ matrices we finally get

$$\Sigma(p) = g^2 \int \frac{d^3k}{(2\pi)^3} \frac{\Sigma(k)}{(k_0^2 + \mathbf{k}^2 + \Sigma^2(k))} \left(1 + \frac{2e^2 B^2 \mathbf{k}^2}{(\Sigma^2 + k^2)^3}\right) \frac{1}{(p-k)^2(1 - N_0(p-k))} \left[2 + \frac{N_1(p-k)\frac{(\mathbf{p}-\mathbf{k})^2}{(p-k)^2}}{1 - \left[N_0(p-k) + \frac{(\mathbf{p}-\mathbf{k})^2}{(p-k)^2}N_1(p-k)\right]}\right].$$

(6.17)

Let us now set $p = 0$ and as in the case of the quenched aprroximation let us make the substitution $\Sigma(k) \simeq \Sigma(0) \equiv m$ to get

$$1 = g^2 \int \frac{d^3k}{(2\pi)^3} \frac{\left(1 + \frac{2e^2 B^2 \mathbf{k}^2}{(m^2 + k^2)^3}\right)}{(k_0^2 + \mathbf{k}^2 + m^2)} \frac{1}{k^2(1 - N_0(k))} \left[2 + \frac{N_1(k)\frac{\mathbf{k}^2}{k^2}}{1 - \left[N_0(k) + \frac{\mathbf{k}^2}{k^2}N_1(k)\right]}\right].$$

(6.18)

Now as $k^2 = k_0^2 + \mathbf{k}^2$ and we can use the parametrization $k_0 = k \cos\theta$ and $|\mathbf{k}| = k \sin\theta$. Let us write, using Eq. (6.11),

$$N_0(p) = E(p) + F(p)\sin^2\theta \qquad (6.19)$$

where $E(p) = -(g^2/8p)(1 - 4e^2 B^2/p^4)$ and $F(p) = -5g^2 e^2 B^2/8p^5$. Accordingly, we can rewrite Eq. (6.18) as

$$1 = g^2 \int \frac{dk}{(2\pi)^2} \frac{1}{(k^2+m^2)} \int_0^\pi d\theta \frac{\sin\theta}{(1 - E(k) - F(k)\sin^2\theta)} \left[2 + \frac{N_1(k)\sin^2\theta}{(1 - E_0(k) - [F(k) + N_1(k)]\sin^2\theta)}\right] \left(1 + \frac{2e^2 B^2 k^2 \sin^2\theta}{(m^2 + k^2)^3}\right).$$

(6.20)

The angular integral can be performed by making a change of variables $y = \cos\theta$, so that we end up with

$$1 = \frac{g^2}{\pi^2} \int dk \frac{1}{(k^2+m^2)} \left[\frac{1}{F(k)} \left(\left\{1 + \frac{2e^2 B^2 k^2(b^2+1)}{(k^2+m^2)^3}\right\} \frac{1}{b}\tan^{-1}\left(\frac{1}{b}\right) - 2\frac{e^2 B^2 k^2}{(k^2+m^2)^3}\right) + \frac{e^2 B^2 k^2 N_1(k)}{(k^2+m^2)^3 F(k)(F(k)+N_1(k))}\right.$$
$$\left. - \frac{1}{2(1-E(k))} \left(\left\{1 + \frac{2(b^2+1)e^2 B^2 k^2}{(m^2+k^2)^3}\right\} \frac{b^2+1}{b}\tan^{-1}\left(\frac{1}{b}\right) - \left\{1 + \frac{2(a^2+1)e^2 B^2 k^2}{(m^2+k^2)^3}\right\} \frac{a^2+1}{a}\tan^{-1}\left(\frac{1}{a}\right)\right)\right],$$

(6.21)

where $b^2 \equiv (1-E-F)/F$ and $a^2 \equiv (1-E-F-N_1)/(N_1 + F)$.

However, this equation is difficult to handle, so we prefer instead to expand Eq. (6.20) in powers of $e^2 B^2$ *before* doing the angular integration. After some rather tedious algebraic manipulations we end up with

$$\frac{eB}{g^4} \equiv \frac{f^2}{4\pi^2} = \sqrt{\frac{1-A_0}{T_1 + T_2}}. \qquad (6.22)$$

The quantities appearing on the right hand side are given by the following expressions:

$$A_0 = \frac{2}{\pi\mu} \int_0^\infty dx \frac{x^2}{(x^2+1)[x^2 + h(\mu,x)]}, \qquad (6.23)$$

$$T_1 = \frac{128\pi^3}{3\mu^5} \int_0^\infty dx \frac{x^4}{(x^2+1)^4 h(\mu,x)}, \qquad (6.24)$$

$$T_2 = \frac{128\pi^3}{9\mu^6} \int_0^\infty dx \frac{12x^4 + x^6}{(4+x^2)^3(x^2+1)[h(\mu,x)]^2}. \qquad (6.25)$$

In the above expressions we have used the notations $f \equiv 2\pi(\sqrt{eB}/g^2)$ and $\mu \equiv 2\pi(m/g^2)$, already used in the previous section; moreover, we have employed the expression

$$h(\mu,x) \equiv \frac{1}{\mu}\left[1 + \frac{x^2-4}{2x}\sin^{-1}\left(\frac{x}{\sqrt{x^2+4}}\right)\right].$$

Numerical computation of the integrals yields m/g^2 as a function of $\sqrt{eB}/g^2$, which can be used to produce the lower branch in Fig. 3. This represents the solution of the SD equations in the region of small magnetic fields. (Note that only the small-B part of the curve is depicted.) We see that the dynamically generated mass in this case is substantially smaller than in the previous section. Presumably this reflects the fact that, due to the Pauli principle, the condensate tends to decrease. We note that in the quenched case the back reaction of the fermions is not really felt, so this fact has no consequences in that case.

VII. LATTICE FORMULATION

We now proceed with a description of the lattice formulation of the problem. The lattice action is given by the formulas given below:

$$S = \frac{\beta_G}{2}\sum_{x,\mu,\nu} F_{\mu\nu}(x)F^{\mu\nu}(x) + \sum_{n,n'} \bar{\Psi}_n Q_{n,n'}\Psi_{n'} \quad (7.1)$$

$$F_{\mu\nu}(x) \equiv a_\mu^S(x) + a_\nu^S(x+\mu) - a_\mu^S(x+\nu) - a_\nu^S(x)$$

$$Q_{n,n'} = \delta_{n,n'} - K\sum_{\hat{\mu}}\left[\delta_{n'n+\hat{\mu}}(r+\gamma_{\hat{\mu}})U_{n\hat{\mu}}V_{n\hat{\mu}}\right.$$
$$\left. + \delta_{n',n-\hat{\mu}}(r-\gamma_{\hat{\mu}})U^\dagger_{n-\hat{\mu},\hat{\mu}}V^\dagger_{n-\hat{\mu},\hat{\mu}}\right].$$

The indices n,n' consist actually of three integers each, (n_1, n_2, n_3), labeling the lattice sites, while μ denotes directions. r is the Wilson parameter, K the hopping parameter, $U_{n\hat{\mu}} \equiv e^{iga\alpha_{n\hat{\mu}}^S}$, $V_{n\hat{\mu}} \equiv e^{ieaA_{n\hat{\mu}}}$. $\alpha_{n\hat{\mu}}^S$ represents the statistical gauge potential and $A_{n\hat{\mu}}$ the external electromagnetic potential. $\beta_G \equiv 1/g^2 a$ is related to the statistical gauge coupling constant in the usual way. On the other hand, we denote by e the dimensionless electromagnetic coupling constant of the external electromagnetic field. In our treatment we will use naive fermions, so we set $r=0$. Initially we will consider a homogeneous magnetic field; thus one should construct a lattice version of the homogeneous magnetic field. This has already been done before in [29] in connection with the Abelian Higgs model. We more or less follow them, but follow a slightly different prescription, which we describe below [8].

Since we would like to impose an external homogeneous magnetic field in the (missing) x_3 direction, we choose the external gauge potential in such a way that the plaquettes in the x_1x_2 plane equal B, while all other plaquettes equal zero. One way in which this can be achieved is through the choice: $A_3(n_1,n_2,n_3) = 0$, for all n_1, n_2, n_3, and

$$A_1(n_1,n_2,n_3) = -\frac{B}{2}(n_2-1), n_1 \neq N, A_1(N,n_2,n_3)$$

$$= -\frac{B}{2}(N+1)(n_2-1), \quad (7.2)$$

$$A_2(n_1,n_2,n_3) = +\frac{B}{2}(n_1-1), n_2 \neq N, A_2(n_1,N,n_3)$$

$$= +\frac{B}{2}(N+1)(n_1-1). \quad (7.3)$$

where N^3 is the number of points on the (cubic) lattice. It is trivial to check out that all plaquettes starting at (n_1,n_2,n_3), with the exception of the one starting at (N,N,n_3), equal B. The latter plaquette equals $(1-N^2)B = B - (N^2B)$. One may say that the flux is homogeneous over the entire x_1x_2 cross section of the lattice and equals B. The additional flux of $-(N^2B)$ can be understood by the fact that the lattice is a torus, that is a closed surface, and the Maxwell equation $\nabla \cdot \boldsymbol{B} = 0$ implies that the magnetic flux through the lattice should vanish. This means that, if periodic boundary conditions are used for the gauge field, the total flux of any configuration should be zero, so the (positive, say) flux B, penetrating the majority of the plaquettes, will be accompanied by a compensating negative flux $-(N^2B)$ in a single plaquette. This compensating flux should be "invisible," that is it should have no observable physical effects. This is the case if the flux is an integer multiple of 2π: $N^2B = m2\pi \rightarrow B = m(2\pi/N^2)$, where m is an integer. Thus we may say (disregarding the "invisible" flux) that the magnetic field is homogeneous over the entire cross section of the lattice.[3] The integer m may be chosen to lie in the interval $[0,N^2/2]$, with the understanding that the model with integers m between $N^2/2$ and N^2 is equivalent to the model with integers taking on the values N^2-m, which are among the ones that have already been considered. It follows that the magnetic field strength B in lattice units lies between 0 and π. The physical magnetic field B_{phys} is related to B through $B = e\alpha^2 B_{phys}$, and the physical field may go to infinity letting the lattice spacing α go to zero, while B is kept constant.

An important remark is that the magnetic field is not allowed to be too big in lattice units, since then the perturbative expansion of the expressions $e^{ieaA_{n\mu}}$ would yield significant B^2, B^3, . . . contributions with the accompanying vertices, in addition to the desirable terms which are linear in B. A trivial estimate of the critical field strength is obtained from the demand that the cyclotron radius corresponding to a given magnetic field should not be less than (say) two lattice spacings. This trivial calculation yields $B < \pi/8$. Of course the above limitations apply strictly only to the case where the statistical gauge field has been turned off; in the "interacting" case, one does not really know whether there exists a critical magnetic field, after which discretization effects are important. With this remark in mind, we depict in the figures of the following sections the results for the whole range of the magnetic field, from 0 to π.

For the fermion fields we used antiperiodic boundary conditions in the time direction and "fixed" boundary condi-

---

[3]To check this translational invariance we measured the fermion condensate at every point in the x_1x_2 plane. The results were the same at all points within the error bars, confirming homogeneity.
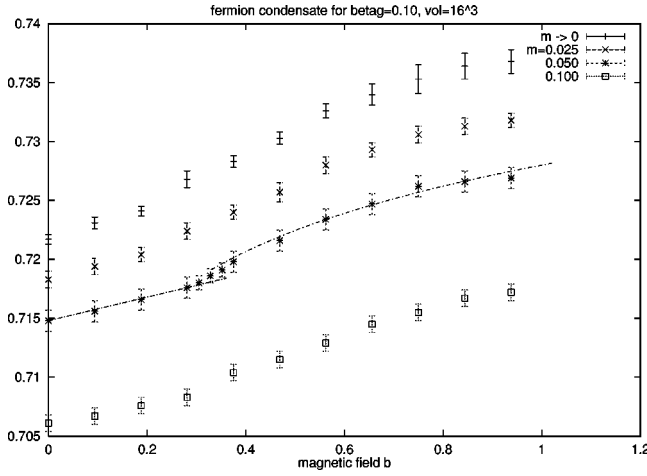
FIG. 4. $\langle \bar{\Psi} \Psi \rangle$ versus the magnetic field strength at strong coupling for three masses and extrapolation to the zero mass limit.

FIG. 5. $\langle \bar{\Psi} \Psi \rangle$ versus magnetic field strength at intermediate coupling for three masses.

tions in the spatial directions; the latter boundary conditions mean that we consider fermion fields vanishing on the boundaries.

VIII. LATTICE RESULTS

A. Zero temperature results

We are now going to present the results pertaining to the $T=0$ case. The first set consists of measurements of the fermion condensate versus the magnetic field for a 16^3 lattice in the strong coupling regime for the statistical gauge field ($\beta_G = 0.10$) for three values of the bare mass (Fig. 4). Before going on with the specific features of these results, let us remark that to facilitate comparison with the analytic results we measured the magnetic field in units of its maximal value: thus we used the parameter b, defined by: $b \equiv B/B_{max} = eB_{phys}a^2/eB_{phys}a^2|_{max}$. Since $B_{max} = \pi$, as explained previously, we get: $b = B/\pi$ and b runs from 0 to 1. We see in Fig. 4 that for all three masses the plot consists of two parts with qualitatively different behavior. For b smaller than about 0.3 we find a dependence of the condensate on the external magnetic field, which is nearly linear, however, in view of the analytical results obtained in Sec. V about the quenched case, we understand that we see the quadratic behavior found there; however, there is a negative quartic term coming into the game, as we also saw, and this "straightens out" the quadratic curve and makes it almost linear. For big magnetic fields we find points that could possibly be fitted to a logarithmic type of curve. The logarithmic dependence

$$\frac{\Sigma(0)}{\alpha} \simeq \ln \left[\frac{\sqrt{eB}}{\alpha} \right], \quad \alpha \equiv \frac{g^2}{4\pi},$$

has been found [12] by an approximate solution of the Schwinger-Dyson equations in the regime of strong magnetic fields. We have included such a logarithmic fit for $m = 0.050$ in Fig. 4. In addition, for this mass some points in the intermediate region are included. They show a smooth interpolation between the two regions. Thus in both the
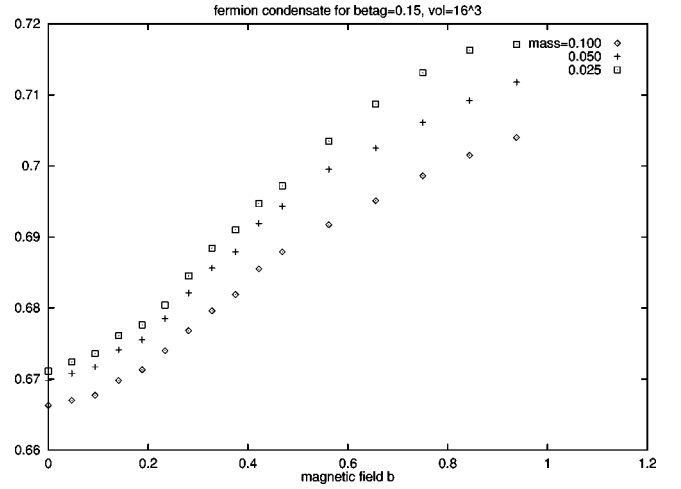
strong and weak magnetic field regimes we find a nice qualitative agreement of the analytical solutions with the Monte Carlo results. In the figure we have also included the extrapolation to the zero mass limit.

The magnetic field has been characterized as "strong" or "weak" through its comparison with the fine structure constant $\alpha \equiv g^2/4\pi$ and the dynamically generated mass $m \simeq \Sigma(0)$. Since Fig. 4 contains the strong coupling data, it would be interesting to explore the fate of the whole picture shown in Fig. 4 as the gauge coupling g moves away from the strong coupling regime. One would naively expect that the magnetic fields will be more easily characterized as "strong," as compared to the smaller and smaller scale set by the gradually weaker coupling constant. Thus, the almost linear part should be restricted to the very small magnetic fields and eventually disappear. This is what one may see in Fig. 5, which is similar to Fig. 4, the only difference being that the gauge coupling constant is now in the intermediate coupling regime, rather than the strong coupling of Fig. 4. We see that the almost linear part is now restricted in the region between $b=0$ and $b \approx 0.12 - 0.15$. We may also have a semi-quantitative estimate of the new "critical" magnetic field b_c, defined as the maximum b which fits into the almost linear behavior. Inspired by the inequality $eB \ll (g^2/4\pi)^2$, let us suppose that $eB_c = x(g^2/4\pi)^2$, with x a very small number; we also make the further assumption that x does not depend on g. We will check crudely whether this assumption is reasonable given our results. Converting everything to lattice units, we find that $b_c = (x/16\pi^3)(1/\beta_G^2)$. From this we infer $b_{c_2} = b_{c_1}(\beta_{G_1}/\beta_{G_2})^2$. Using $\beta_{G_1} = 0.10$, $\beta_{G_2} = 0.15$ and $b_{c_1} = 0.3$, we find for b_{c_2}, the value 0.13, which is surprisingly close to the value given by the data of Fig. 5. Of course, the $1/\beta_G^2$ dependence of b_c tells us that the weak field behavior will be even more suppressed as we move towards the weak gauge coupling; this is what we have seen in direct simulations in this regime. Thus, it is plausible that the dependence of the "critical" magnetic field has a $1/\beta_G^2$ dependence.
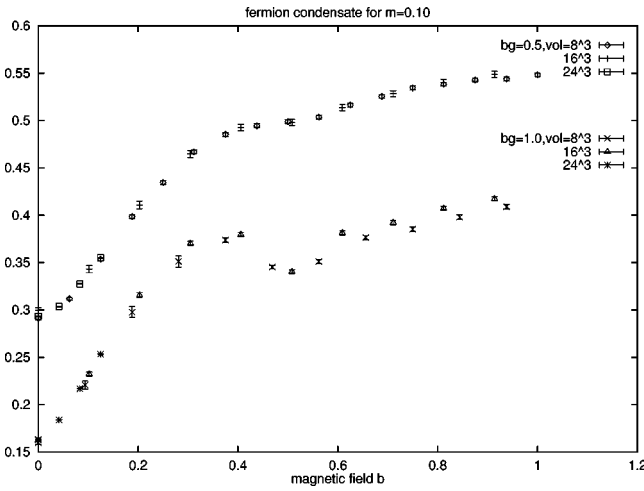
We now make contact with the results of [8], where we

FIG. 6. $\langle \bar{\Psi} \Psi \rangle$ versus the magnetic field for two small values of the gauge coupling constant and three volumes.

FIG. 7. $\langle \bar{\Psi} \Psi \rangle$ versus m for a typical value of the magnetic field strength and various values of β_G.

studied the model with the statistical gauge field turned off. We had found there that for big enough b the condensate stopped showing a monotonous increase with b, at $b=0.5$ it had a local minimum and then had a succession of maxima and minima, up to $b=1$. Moreover, there was a spectacular volume dependence. One expects, of course that this ''free'' case will be reached for big enough β_G. In Fig. 6 we show the results for $\beta_G=0.5$ and $\beta_G=1.0$ for various volumes. For $\beta_G=0.5$ the curve shows the first sign of non monotonous behavior at $b=0.5$, while at $\beta_G=1.0$ the succession of maxima and minima is clear. However, there is no detectable volume dependence, so we can be sure that, even at this large β_G, the limit of switching the gauge field off has not yet been reached; it will presumably be reached for even bigger values of β_G. One should add that in the ''free'' case the role of the bare mass is very important, since it is eventually the only source of mass generation. This is at the root of the large volume dependence showing up in the ''free'' case: at fixed volume the condensate goes over to zero for vanishing bare mass. In the full model, though, the interaction with the gauge field generates a dynamical mass, independently from the value of the bare mass. This is why in the ''interacting'' case the volume dependence is small, permitting a smooth transition to the thermodynamic, as well as to the massless, limit.

The simulations are done at finite values for the (bare) mass; the massless limit is taken by extrapolating the results for several bare masses to the limit $m \rightarrow 0$. Figure 7 shows the process of this extrapolation for three values of the gauge coupling constant. The external magnetic field has been set equal to a typical value ($b=0.188$); the picture is similar for all values of the magnetic field strength. For $\beta_G=0.10$, which lies in the strong coupling region, the extrapolation is linear with negative slope. This line is pointing to a relatively big value for the condensate in the chiral limit. For somewhat weaker coupling ($\beta_G=0.20$), the curve is still a straight line, but the slope is positive and it points to a smaller value at $m \rightarrow 0$. In both of these cases the mass dependence is not very pronounced, because it is the strong
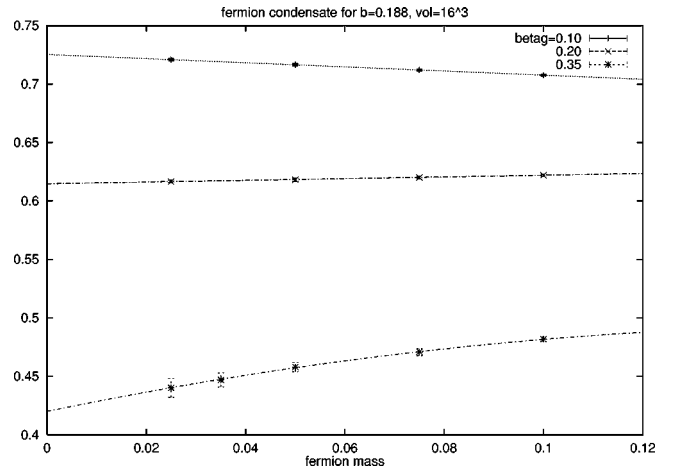
gauge coupling which dominates in the formation of the condensate. In the third case ($\beta_G=0.35$), which lies in the weak coupling, one can no longer fit to a straight line; a quadratic fit has proved necessary for all β_G values smaller than 0.2.

Figure 8 contains the zero mass limit of the condensate (obtained through the procedure illustrated in Fig. 7) versus β_G, for four values of the external field. We observe that in the strong coupling region the b-dependence of the condensate is rather weak; on the contrary, at weak coupling, the external field is the main generator of the condensate, and we find an increasingly big b-dependence, as we move to large β_G. Note that the biggest value of b we have used in systematic measurements, such as the ones in Fig. 8, is 0.3. This takes into account that for larger values of b the function of the condensate stops being monotonous for large β_G, as may be seen on Fig. 6. Thus we have restricted our study to a b region which is safe for all values of the coupling. From this preliminary quenched study we conclude that a nonvanishing value for $\langle \bar{\Psi} \Psi \rangle$ develops for this small volume even at weak coupling in the presence of an external mag-
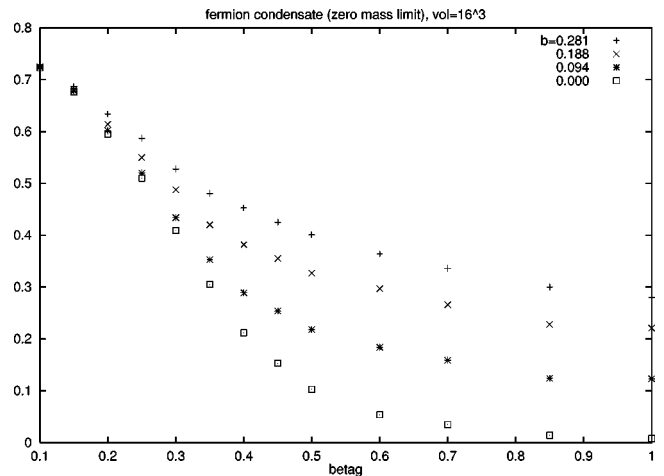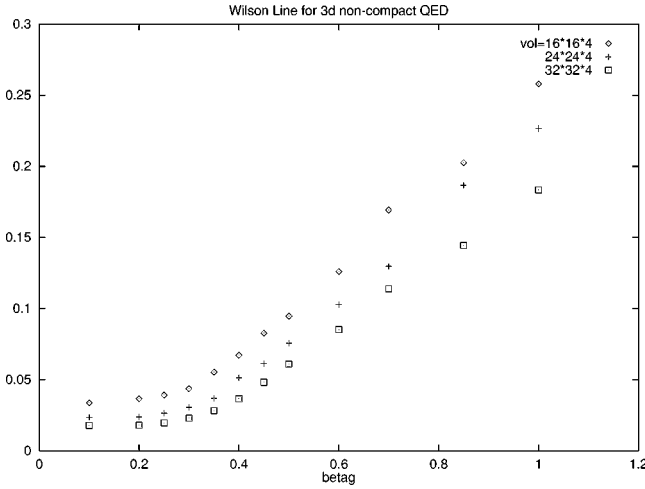

FIG. 8. $\langle \bar{\Psi} \Psi \rangle$ versus β_G n the zero mass limit for four values of the magnetic field strength.

FIG. 9. Wilson line versus β_G for $N_\tau = 4$ and three spatial sizes.

FIG. 11. Condensate versus β_G for b=0.1. Comparison of zero temperature with finite temperature.
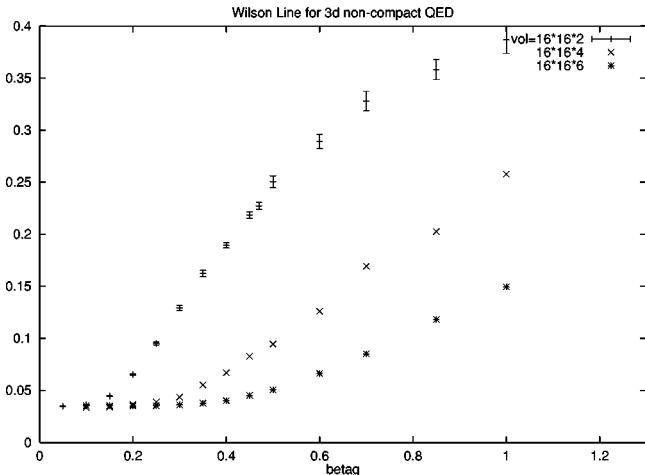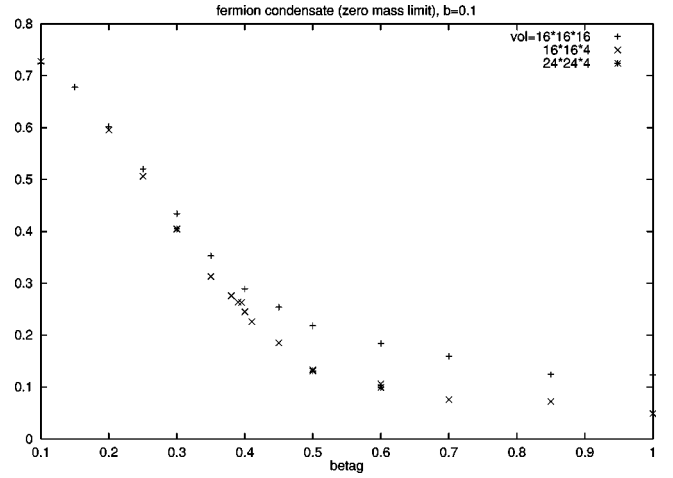
netic field. We have not tried to study systematically the approach to the continuum limit.

B. Finite temperature results

We expect that the fermion condensate, generated by any mechanism (explicit mass term, gauge interactions, external fields) should vanish at high temperatures. This is the study we now turn to: we employ asymmetric lattices and consider the behavior of the condensate versus β_G. Before describing the behavior of the condensate, let us first see the β_G dependence of the Wilson line.

Figure 9 depicts the Wilson line versus β_G for lattices of temporal size $N_\tau = 4$ and various spatial volumes. We observe in the figure not only the decrease of the Wilson line with increasing spatial volume, but also the fact that initially this quantity is almost independent of β_G, but at $\beta_G \simeq 0.25$ its dependence on β_G starts showing up. It is important that this value of β_G is independent from the spatial volume.

In Fig. 10 we show the relationship between Wilson lines on lattices with $N_\tau = 2$ versus $N_\tau = 4$ and $N_\tau = 6$. The result for the $16^2 \times 6$ lattice lies ''below'' the result for the 16^2

FIG. 10. Wilson line versus β_G for $N_\tau = 2$, $N_\tau = 4$ and $N_\tau = 6$.

$\times 4$. This is due to the fact that the former lattice is closer to the zero temperature (symmetric) lattices, as compared to the latter. The value of β_G, above which there is β_G dependence is substantially bigger for $N_\tau = 6$ than for $N_\tau = 4$ or $N_\tau = 2$. The Wilson line for the $N_\tau = 2$ case approaches an asymptotic value for large β_G. This is not very obvious in the other two cases, because they lie farther from the infinite temperature limit. Also in this case the statistical fluctuations are very large, resulting in big errors. With this in mind we have put in the figure only the errors for the case $N_\tau = 2$.

Figure 11 contains the zero (bare) mass extrapolations for the condensate as a function of β_G. The external magnetic field is set to $b = 0.1$. The uppermost curve contains the results for a symmetric lattice (16^3.) It is easily seen that it is a quite smooth curve and presents no apparent discontinuities of any sort. The data for the asymmetric lattice $16^2 \times 4$ follow the ones of the symmetric lattice at strong coupling; in the weak coupling region the condensate for the asymmetric lattice appears substantially smaller than its 16^3 counterpart. This is what one should explain on account of the symmetry restoration scenaria at finite temperatures. The $16^2 \times 4$ data can be described by two branches, one containing the strong and the other the weak coupling results; the two branches join at about $\beta_G = 0.4$, but their slopes do not coincide. There is a discontinuity at this value of β_G, which we interpret as the symmetry restoring transition at finite temperature. On the same figure we have put the results for a lattice of bigger spatial volume ($24^2 \times 4$), away from the ''critical'' $\beta_G = 0.4$ value. These data do not differ substantially from the ones for $16^2 \times 4$.

Figure 12 contains results similar to the ones of Fig. 11, but the value of the external magnetic field differs: $b = 0.305$. The same basic picture appears here, as well: we may again spot the discontinuity at $\beta_G = 0.4$ for $N_t = 4$. In addition to the data of Fig. 11 we have put the data for a $24^2 \times 6$ lattice, which is expected to lie closer to zero temperature. The data are smoother than the ones for $16^2 \times 4$ and they lie much closer to the 16^3 results; this makes it more difficult than before to spot a sudden change in slope; however, this change is present even in this case. The new ele-
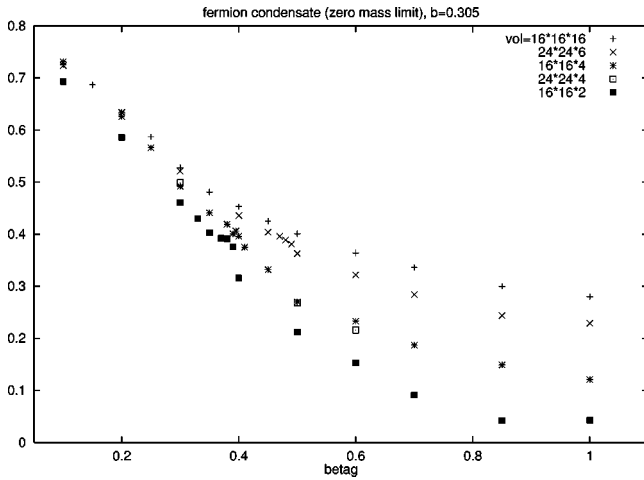
FIG. 12. Condensate versus β_G for b=0.3. Comparison of zero temperature with finite temperature. The error bars (not shown) are almost of the size of the symbols.

ment here is the data for $N_t=2$. The change in slope here is very pronounced and substantiates our claim that we have a phase transition around $\beta_G=0.4$.

Since we now have data for several asymmetric lattices, we are in a position to show the temperature dependence of the condensate. This is done in Fig. 13, in the weak coupling regime, for two values of the magnetic field. The zero mass extrapolation of the results has been used and the temperature in lattice units is $1/N_t$, as usual. We observe the fall of the condensate at high temperatures, which is more dramatic for the smallest value of b. This figure is of the same qualitative form with Figure 2 of [8], which was derived analytically for the case where we had no statistical gauge field at all.

In Fig. 14 we show the time evolution of the condensate for two values of the magnetic field at weak coupling for a symmetric lattice. The important feature here is the very small magnitude of the statistical fluctuations, resulting in relatively small errors.
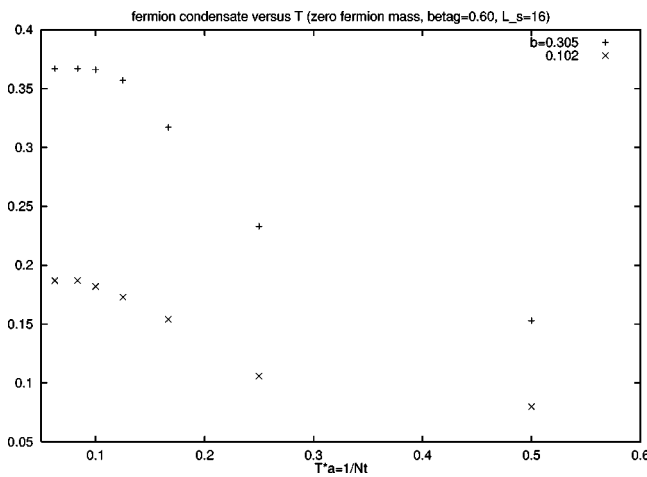

FIG. 13. $\langle \bar{\Psi}\Psi \rangle$ versus the temperature for two values of the magnetic field.
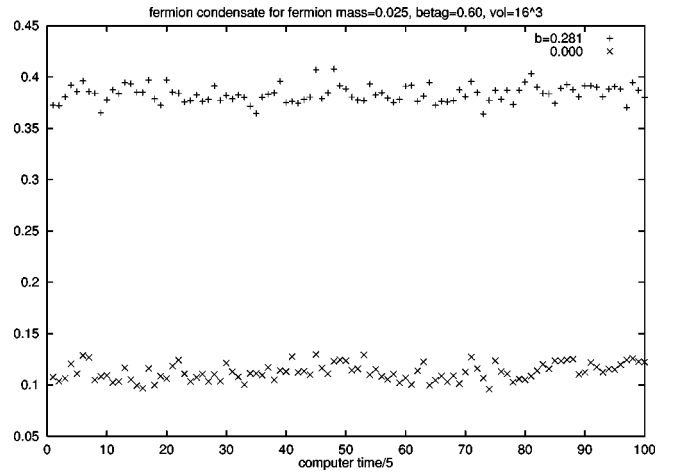

FIG. 14. Time evolution of $\langle \bar{\Psi}\Psi \rangle$ for a symmetric (16^3) lattice and two values of the magnetic field.

The situation in Fig. 14 changes in the asymmetric lattices and the results of Fig. 14 should be contrasted against the ones in Figs. 15 and 16. In Fig. 15 we have exactly the same parameters as in Fig. 14, however now we have a $16^2 \times 4$ lattice. It is evident that the fluctuations have grown about one order of magnitude larger.

The statistical fluctuations grow even larger for the $16^2 \times 2$ lattice, whose results are shown in Fig. 16. Moreover, this figure gives a feeling of the way the average of the condensate is approaching zero at high enough temperatures. The outcome spends most of its time at small values and has some exceptional big spikes from time to time; these latter become more and more rare as the spatial volume increases.

C. Non-uniform magnetic field

In the previous sections we have considered the case of a uniform external magnetic field. There is however potential physical interest in the effects of non-uniform fields, which become important in case the above model has relevance to the physics of high-temperature superconductors. Indeed, it will be of interest to examine the effect of electromagnetic
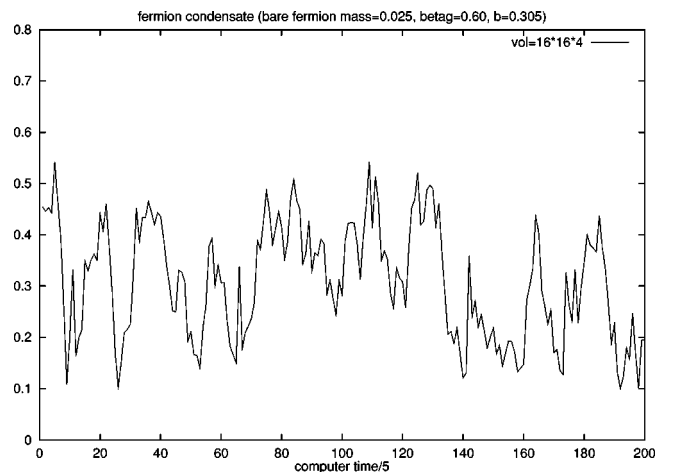

FIG. 15. Time evolution of $\langle \bar{\Psi}\Psi \rangle$ for a $16^2 \times 4$ lattice.
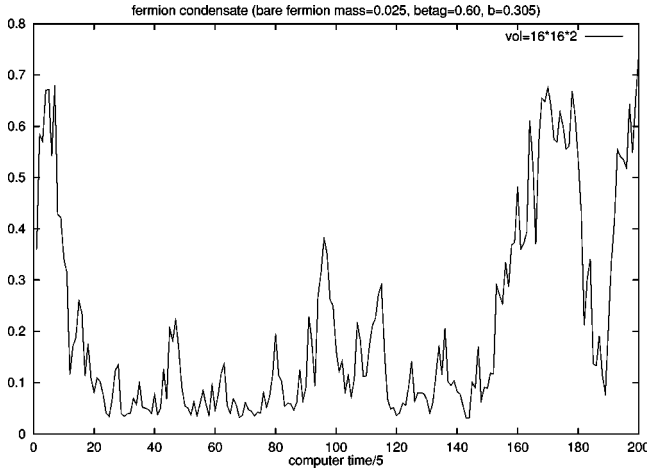
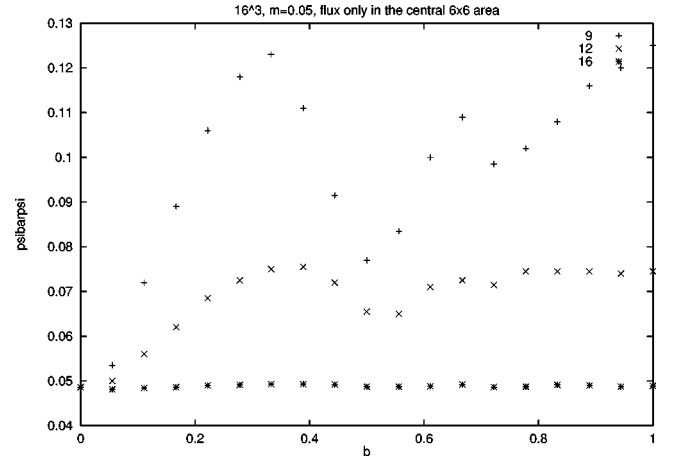FIG. 16. Time evolution of $\langle\bar{\Psi}\Psi\rangle$ for a $16^2\times 2$ lattice.

FIG. 17. $\langle\bar{\Psi}\Psi\rangle$ versus magnetic field strength where the flux is non zero only in a central region extending over 6×6 plaquettes. The condensate at sites labeled 9, 12, 16 (see text) is shown. The corresponding distances from the center of the flux tube are 0, 3, 7.

vortex lines on the induced fermion (holon) condensate at the nodes of d-wave superconducting gaps [7]. A simple-minded model for such vortex lines could be that of flux tubes of magnetic field. The full problem would be to take into account interactions among the flux tubes, which could shed light also in the confining aspects of the gauge groups in three dimensions. It is only by lattice methods that one may treat the problem, in view of the very big computational difficulties in the analytical approach. In this first treatment of the problem we switch off the fluctuating statistical gauge field and consider the response of the fermions to the background field only. A full treatment of the problem, including the statistical gauge interactions is left for the future.

Let us describe the technical procedure to construct a non-uniform magnetic field on the lattice. We will consider $M\times M$ plaquettes parallel to the x_1x_2 plane, around the center of the lattice, which will be penetrated by magnetic flux equal to B each. The remaining plaquettes will not carry any flux. Then we are going to measure the condensate at the center $(N/2,N/2,N/2)$ and along a line passing through it and consisting of the sites $(N/2,N/2+1,N/2)$, $(N/2,N/2+2,N/2)$, ..., $(N/2,N,N/2)$.

The fact remains that the total flux through the lattice should be zero, because of div $\mathbf{B}=0$. Thus, for each flux B penetrating a given plaquette, there should be an opposite flux somewhere else in the lattice. To construct the magnetic field that we mentioned above, we followed the strategy to build it up plaquette by plaquette taking care that we put the compensating opposite flux through the plaquette starting at the point (N,N,n_3). If we already have a configuration of gauge potentials on a lattice, the procedure to add a plaquette of flux B at the plaquette at (N_1,N_2,n_3) (with the corresponding compensating flux $-B$ at (N,N,n_3)), consists of adding to the preexisting links the quantities denoted by ΔA_k below. $\Delta A_3(n_1,n_2,n_3)$ is set to zero for all values of the integers n_1,n_2,n_3. ΔA_1 and ΔA_2 are also set to zero, except for the links where an explicit different statement is made. For the plaquette starting at the site $(N_1,N_2,n_3),N_1\neq N,N_2\neq N$, we choose

$$\Delta A_1(N_1,n_2,n_3)=-B, \quad n_2=N_2+1,N_2+2,\ldots,N,$$

$$n_3=1,\ldots,N$$

$$\Delta A_2(n_1,N_2,n_3)=+B, \quad n_1=N_1+1,N_1+2,\ldots,N,$$

$$n3=1,\ldots,N.$$

For $N_1=N$ we impose

$$\Delta A_1(N,n_2,n_3)=-B, \quad n_2=N_2+1,N_2+2,\ldots,N,$$

$$n_3=1,\ldots,N$$

$$\Delta A_2(n_1,n_2,n_3)=0 \quad \text{everywhere,}$$

while for $N_2=N$

$$\Delta A_1(n_1,N,n_3)=0 \quad \text{everywhere,}$$

$$\Delta A_2(n_1,N,n_3)=B, \quad n_1=N_1+1,N_1+2,\ldots,N,$$

$$n_3=1,\ldots,N.$$

In the following we consider the model with the statistical gauge field turned off. We start with vanishing gauge potentials everywhere on the lattice, go through the plaquettes in the central region and add the above ΔA_k quantities to the corresponding links. In this way we end up with the flux B in the central plaquettes and the compensating flux for all the plaquettes at (N,N,n_3). The flux through these latter plaquettes should be "invisible," as explained in Sec. VII, so B must take the values $(2\pi/M^2)n$, $n=0,1,\ldots,M^2/2$.

In Fig. 17 we show the results for a central region of non-vanishing flux of extent 6×6. More specifically, for the 16^3 lattice we have been using, the region with constant non-zero flux contains the plaquettes starting at (n_1,n_2,n_3), with $6\leqslant n_1\leqslant 11$ and $6\leqslant n_2\leqslant 11$, while n_3 takes all values. Note that nothing depends on the value of n_3. The uppermost curve in the figure depicts the result for the condensate at the site $(9,9,9)$. The remaining curves represent the correspond-
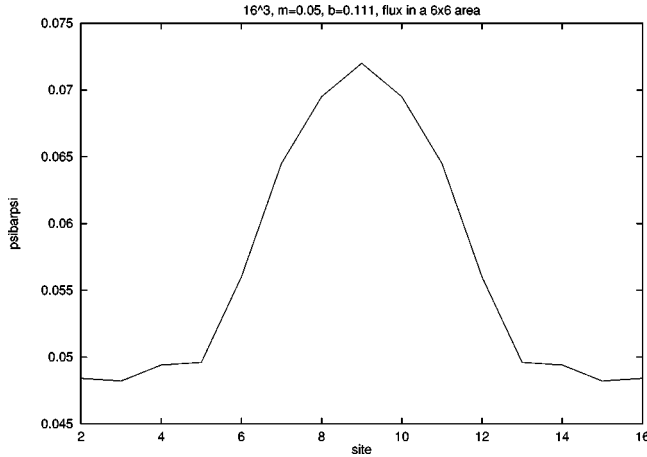
FIG. 18. $\langle \bar{\Psi} \Psi \rangle$ along a straight line passing from the center of the lattice if the magnetic field parameter b is set to 0.111. The central region of non-zero flux is 6×6.

ing results for the sites (9,12,9), and (9,16,9). The curves with $n_2 = 10$, $n_2 = 11$ are quite similar to the $n_2 = 9$ curve. The first substantial change takes place at the site (9,12,9), which lies exactly on the boundary of the above region. The remaining curves dive together to a value which is accounted for by the explicit mass term and has very little to do with the external magnetic field. Thus, we find a drop in the condensate value taking place exactly on the boundary of the central region.

To visualize the fall of the condensate on the boundary, we fixed the b parameter to 0.111 (a typical value) and plotted the value of the condensate along a straight line passing from the center of the lattice. We find the symmetric bell-shaped plot shown in Fig. 18.

IX. CONCLUSIONS

In this work we have studied in detail, by means of analytic and lattice methods, the phenomenon of magnetic catalysis in even-flavor QED$_3$, namely the magnetic induction of a chiral-symmetry breaking fermion condensate as a result of the influence of an external magnetic field. We have shown that the scaling behavior of the induced condensate with the external field varies according to the strength of the latter. In the weak-field regime, there is a quadratic increase of the condensate with increasing external field, to be contrasted with the logarithmic scaling behavior in the regime of strong external magnetic fields. However, it seems that the transition from weak to strong fields is smooth, at least as far as the induced condensate is concerned, and we would characterize it as a *cross-over* rather than a phase transition at some critical value of the external field. This constitutes a prediction of the gauge theory, and it may be tested in experiments of relevance to high-temperature superconducting materials. It would be interesting to repeat the (lattice) computations for the case of four-fermion contact interactions to check on this behavior. This would differentiate between the two models as possible candidates for the *nodal* spin-charge excitations in *d*-wave high-temperature superconductors [7,15].

It should be stressed that the analytic methods that lead to this scaling are approximate, and should be considered only as giving a qualitative treatment of the phenomenon. The important effect of the external field is the breaking of translational invariance on the spatial plane, and this leads to technical complications in solving the pertinent Schwinger-Dyson equations in the case of weak magnetic fields, mixing configuration and momentum space integrals. To bypass this problem, we adopted an ansatz for the fermion propagator in the presence of a weak external field, which although maintains formally a translational invariant look (in the sense of its being expressed in terms of a Fourier transform depending on a single momentum variable), however it incorporates the effects of the magnetic field in the pertinent coefficients. Comparison with the quenched lattice results showed that the predicted scaling of the induced condensate with the magnetic field is (qualitatively) captured by this ansatz.

In addition to the uniform external field case, we have also presented preliminary quenched lattice results in the case of flux tubes of magnetic field. This situation might also be of relevance to realistic situations in high-temperature superconductors, as being related to the effects of electromagnetic vortex lines on the opening of a fermion gap at the nodes of the superconductor, within the context of the gauge theory approach [7]. Our results in the non-uniform magnetic field case have indicated that the fermion chiral condensate is non zero and scales with the magnetic field of the flux tube at the core of the latter, but decays very fast outside the tube. Our considerations did not properly take into account interactions among flux tubes. The latter is an important issue, which might also bear some relation with the issue of confinement of the three-dimensional theory. We expect that a proper treatment of this problem will become available only upon the use of dynamical fermions on the lattice.

Another important issue we would like to address for future work is the computation of thermal conductivities in the context of the model of Sec. II, used in our simulation of the physics of planar high-temperature superconductors. As discussed in [14] there are scaling differences of the thermal conductivity between the gauge (QED$_3$) and four-fermion models, which would be important to analyze in detail in the context discussed in this work for comparison with experiments of high-temperature superconductors [13]. At present, the analysis of the thermal conductivity has been performed in the real time formalism [15,14], and the extension to a lattice analysis is not trivial. We hope to return to this important issue in a future publication.

APPENDIX A: CALCULATION OF THE ONE-LOOP VACUUM POLARIZATION IN THE PRESENCE OF THE EXTERNAL MAGNETIC FIELD

The photon polarization tensor for QED in the presence of the electromagnetic field was first performed by Tsai [30,31]. Here, for the sake of completeness, we outline his calculations but we will work in three-dimensions instead of four-dimensions.

Let us begin with the one-loop vacuum polarization graph (2). The polarization tensor to this approximation is given by

$$\Pi_{\mu\nu}(p) = -g^2 \int \frac{d^3k}{(2\pi)^3} \text{tr}[\gamma^\mu \widetilde{S}(k)\gamma^\nu \widetilde{S}(p-k)] \quad \text{(A1)}$$

where the Fermion propagator is the one in the presence of the constant external magnetic field [10]

$$\widetilde{S}_F(k) = i \int_0^\infty ds\, e^{-s(k_0^2+m^2+\mathbf{k}^2(\tanh z/z))}[(m-\gamma\cdot k) - i(\gamma_1 k_2 - \gamma_2 k_1)\tanh z](1-i\gamma_1\gamma_2\tanh z)$$

$$= i \int_0^\infty ds\, e^{-s(m^2+k_0^2+\mathbf{k}^2(\tanh z/z))} \left((m-\gamma_0 k_0)(1-i\gamma_1\gamma_2\tanh z) - (\gamma\cdot k)\frac{1}{\cosh^2 z} \right) \quad \text{(A2)}$$

where $z \equiv eBs$. Accordingly, Eq. (A2) leads us to

$$\Pi_{\mu\nu}(p) = -g^2 \int \frac{d^3k}{(2\pi)^3} \int_0^\infty ds_1 \int_0^\infty ds_2\, e^{-(\chi_0(s_1,k)+\chi_0(s_2,p-k))}$$

$$\times \text{tr}\left[\gamma^\mu \left((m-\gamma_0 k_0)(1-i\gamma_1\gamma_2\tanh z_1) - (\gamma\cdot k)\frac{1}{\cosh^2 z_1} \right) \right.$$

$$\left. \times \gamma^\nu \left([m-\gamma_0(p-k)_0](1-i\gamma_1\gamma_2\tanh z_2) - [\gamma\cdot(p-k)]\frac{1}{\cosh^2 z_2} \right) \right] \quad \text{(A3)}$$

where $z_i = eBs_i$, $i=1,2$ and

$$\chi_0(s,k) \equiv s\left(m^2 + k_0^2 + \mathbf{k}^2 \frac{\tanh z}{z} \right). \quad \text{(A4)}$$

Let us now make the change of variables

$$s_1 \equiv \frac{1-v}{2}s, \quad s_2 = \frac{1+v}{2}s, \quad \text{(A5)}$$

with $s \in [0,\infty)$ and $v \in [-1,1]$. Accordingly, we get

$$\chi_0(s_1,k) + \chi_0(s_2,p-k) = s[\phi_0(p) + \phi_1(p,k)] \quad \text{(A6)}$$

with

$$\phi_0(p) \equiv m^2 + \frac{1-v^2}{4}p_0^2 + \frac{\cosh z\, v - \cosh z}{2z \sinh z}\mathbf{p}^2$$

$$\phi_1(p,k) \equiv \left(k_0 - \frac{1+v}{2}p_0 \right)^2 + \frac{\tanh z_1 + \tanh z_2}{z}$$

$$\times \left(\mathbf{k} - \frac{\tanh z_2}{\tanh z_1 + \tanh z_2}\mathbf{p} \right)^2. \quad \text{(A7)}$$

The loop integrals can then be performed very easily via standard Gaussian integrations some of which are listed below:

$$I_0 \equiv \int \frac{d^3k}{(2\pi)^3} e^{-s\phi_1(p,k)} = \frac{1}{(4\pi s)^{3/2}}\frac{z}{\sinh z}\cosh z_1 \cosh z_2 \quad \text{(A8)}$$

$$\int \frac{d^3k}{(2\pi)^3} e^{-s\phi_1(p,k)} k_0 = \frac{1+v}{2}p_0 I_0 \quad \text{(A9)}$$

$$\int \frac{d^3k}{(2\pi)^3} e^{-s\phi_1(p,k)} \mathbf{k} = \frac{\tanh z_2}{\tanh z_1 + \tanh z_2}\mathbf{p} I_0 \quad \text{(A10)}$$

$$\int \frac{d^3k}{(2\pi)^3} e^{-s\phi_1(p,k)} k_0 \mathbf{k} = \frac{1+v}{2}\frac{\tanh z_2}{\tanh z_1 + \tanh z_2} I_0 p_0 \mathbf{p} \quad \text{(A11)}$$

$$\int \frac{d^3k}{(2\pi)^3} e^{-s\phi_1(p,k)} k_i k_j = \left[\left(\frac{\tanh z_1}{\tanh z_1 + \tanh z_2} \right)^2 p_i p_j \right.$$

$$\left. - \frac{z}{s(\tanh z_1 + \tanh z_2)}\delta_{ij} \right]. \quad \text{(A12)}$$

We will also need the following identity for the gamma matrices:

$$\text{tr}[(1 - i\gamma_1\gamma_2\tanh z)\gamma_\mu\gamma_\nu]$$

$$= -4(\delta_{\mu\nu} - \tanh z(\delta_1^\mu\delta_2^\nu - \delta_1^\nu\delta_2^\mu))$$

$$= -4\left(\delta_{\mu\nu} - \tanh z\frac{F_{\mu\nu}}{B}\right) \qquad (A13)$$

where $F_{\mu,\nu}$ is the covariant representation of the external magnetic field strength. The other traces can also be evaluated by the use of the Dirac algebra (2.6).

Putting everything together [30,31] one gets (after an integration by parts)

$$\Pi_{\mu\nu}(p) = \frac{g^2}{\sqrt{2\pi}}\int\frac{ds}{\sqrt{s}}\frac{dv}{2}\frac{z}{\sinh z}e^{-s\phi_0}I_{\mu\nu} \qquad (A14)$$

where

$$I_{\mu\nu} = [(\delta_{\mu\nu}p^2 - p_\mu p_\nu)R_0(p) + (\delta_{\mu\nu}^\perp p_\perp^2 - p_{\perp\mu}p_{\perp\nu})R_1(p)] \qquad (A15)$$

with

$$R_0(p) = (\cosh zv - v\coth z\sinh zv) \qquad (A16)$$

$$R_1(p) = \frac{2}{\sinh^2 z}[\cosh z - \cosh zv] - R_0(p). \qquad (A17)$$

Note that, unlike its four-dimensional counterpart, the vacuum polarization tensor in three dimensions is not divergent and there is no need to add any counterterms. One can see this by checking the absence of poles at $s\to 0$, which is the place where poles usually show up in proper time methods.

---

[1] V.P. Gusynin, V.A. Miransky, and I.A. Shovkovy, Phys. Rev. D **52**, 4718 (1995); Nucl. Phys. **B462**, 249 (1996).

[2] C.N. Leung, Y.J. Ng, and A.W. Ackley, Phys. Rev. D **54**, 4181 (1996); D.S. Lee, C.N. Leung, and Y.J. Ng, *ibid.* **55**, 6504 (1997); V.P. Gusynin and I.A. Shovkovy, *ibid.* **56**, 5251 (1997); V.P. Gusynin, hep-ph/9709339.

[3] I.V. Krive and S.A. Naftulin, Phys. Rev. D **46**, 2737 (1992); K.G. Klimenko, Theor. Math. Phys. **89**, 1161 (1992); Z. Phys. C **54**, 323 (1992).

[4] D.K. Hong, Y. Kim, and S.J. Sin, Phys. Rev. D **54**, 7879 (1996).

[5] D.K. Hong, Phys. Rev. D **57**, 3759 (1998).

[6] A.V. Shpagin, hep-ph/9611412.

[7] K. Farakos and N.E. Mavromatos, Int. J. Mod. Phys. B **12**, 809 (1998).

[8] K. Farakos, G. Koutsoumbas, and N.E. Mavromatos, Phys. Lett. B **431**, 147 (1998).

[9] V.P. Gusynin, D.K. Hong, and I.A. Shovkovy, Phys. Rev. D **57**, 5230 (1998).

[10] J. Schwinger, Phys. Rev. **82**, 664 (1951).

[11] N. Dorey and N.E. Mavromatos, Phys. Lett. B **250**, 107 (1990); Nucl. Phys. **B386**, 614 (1992); for a comprehensive review of this approach, see N.E. Mavromatos, Nucl. Phys. B (Proc. Suppl.) **C33**, 145 (1993).

[12] K. Farakos and N.E. Mavromatos, Phys. Rev. B **57**, 3017 (1998).

[13] K. Krishana *et al.*, Science **277**, 83 (1997).

[14] K. Farakos, G. Koutsoumbas, and N.E. Mavromatos, Int. J. Mod. Phys. B **12**, 2475 (1998).

[15] G.W. Semenoff, I.A. Shovkovy, and L.C.R. Wijewardhana, Mod. Phys. Lett. A **13**, 1143 (1998).

[16] R.D. Pisarski, Phys. Rev. D **29**, 2423 (1984); T.W. Appelquist, M. Bowick, D. Karabali, and L. C. R. Wijewardhana, *ibid.* **33**, 3704 (1986); T.W. Appelquist, D. Nash, and L.C.R. Wijewardhana, Phys. Rev. Lett. **60**, 2575 (1988).

[17] I.J.R. Aitchison and N.E. Mavromatos, Phys. Rev. B **39**, 6544 (1989); **53**, 9321 (1996).

[18] P.W. Anderson, Science **235**, 1196 (1987).

[19] N.E. Mavromatos and A. Momen, Mod. Phys. Lett. A **13**, 1765 (1998).

[20] K. Farakos, G. Koutsoumbas, and G. Zoupanos, Phys. Lett. B **249**, 101 (1990).

[21] P.W. Wiegmann, Prog. Theor. Phys. Suppl. **107**, 243 (1992); X.G. Wen and P.A. Lee, Phys. Rev. Lett. **76**, 503 (1996).

[22] J. Frohlich and P. Marchetti, Phys. Rev. B **46**, 6535 (1992); J. Frohlich, T. Kerler, and P. Marchetti, Nucl. Phys. **B374**, 511 (1992).

[23] P.A. Marchetti, Zhao-bin Su, and Lu Yu, Nucl. Phys. **B482**, 731 (1996).

[24] K. Farakos, N.E. Mavromatos, and D. McNeill, Phys. Rev. D **59**, 034502 (1999).

[25] C. Vafa and E. Witten, Commun. Math. Phys. **95**, 257 (1984).

[26] A. Chodos, K. Everding, and D. Owen, Phys. Rev. D **42**, 2881 (1990).

[27] For recent work on the effects of wave-function renormalization, see I.J.R. Aitchison, N.E. Mavromatos, and D. McNeill, Phys. Lett. B **402**, 154 (1997); K-I. Kondo and T. Murakami, *ibid.* **410**, 257 (1997), and references therein.

[28] See, for example, M. Koopmans, Ph.D. thesis, University of Groningen, 1990; V. Gusynin, A. W. Schreiber, T. Sizer, and A.G. Williams, Phys. Rev. D **60**, 065007 (1999).

[29] P.H. Damgaard and Urs M. Heller, Nucl. Phys. **B309**, 625 (1988).

[30] W. Tsai, Phys. Rev. D **10**, 1399 (1974).

[31] W. Dittrich and M. Reuter, *Effective Lagrangian in Quantum Electrodynamics* (Springer-Verlag, Berlin, 1984).